Energy analysis of autoclave CFRP manufacturing using thermodynamics based models

Ogugua, Chizoba J.; Anton, Sabin V.; Tripathi, Aditya P.; Larrabeiti, Miguel Dominguez; van Hees, Sean O.; Sinke, Jos; Dransfeld, Clemens A.

DOI
10.1016/j.compositesa.2022.107365

Publication date
2023

Document Version
Final published version

Published in
Composites Part A: Applied Science and Manufacturing

Composites: Part A 166 (2023) 107365

Contents lists available at ScienceDirect

Composites Part A

journal homepage: www.elsevier.com/locate/compositesa

Energy analysis of autoclave CFRP manufacturing using thermodynamics based models

Chizoba J. Ogugua[1,*], Sabin V. Anton[1], Aditya P. Tripathi[1], Miguel Dominguez Larrabeiti[1], Sean O. van Hees[1], Jos Sinke[2], Clemens A. Dransfeld[3]

Aerospace Manufacturing Technologies, Delft University of Technology, Kluyverweg 1, Delft, 2629 HS, South Holland, The Netherlands

ARTICLE INFO

Keywords:
Energy consumption
Autoclave curing
Composites manufacturing
Lattice Boltzmann
Energy efficiency

ABSTRACT

Autoclave curing is one of the most energy consuming processes in manufacturing carbon fibre reinforced polymers. In order to improve the energy efficiency, one needs to understand energy usage in an autoclave and factors that influence it. This work presents two thermodynamic based models for estimating energy consumption in an autoclave. The first model is an analytical approach based on simplified heat capacity equation. The second model combines the Multi-Relaxation-Time Lattice Boltzmann method (MRT LBM) with Fourier heat equation to simulate autoclave temperature flow and energy consumption. The output from the two models were compared to energy consumption data collected using a power meter. The estimated values from the MRT LBM method showed a better match with only 1% difference from the experimental value. Since the two models are parametric and scalable, a what-if analysis was carried out to investigate the influence of varying process parameters on autoclave energy consumption. Parameters including cure cycle, autoclave size and loading capacity.

1. Introduction

Carbon-Fibre-Reinforced Polymers (CFRP) were introduced into the aviation industry in the early 1960s. Their excellent specific strength and stiffness make them desirable for aerospace applications, as they can lead to weight reductions of aircraft components. Weight reduction in aircraft can lead to improved fuel efficiency during operation. Adopting CFRP materials in aerospace structures could create environmental problems outside the operational phase such as raw material production, manufacturing and end of life. With such widespread use, CFRP part manufacturing processes require additional optimization to minimize their environmental impact to make large-scale production more environmentally friendly.

Autoclave curing is a common curing/consolidation method used for fabricating primary aircraft structures, as it ensures the highest quality of CFRP parts. The controlled pressure and temperature in an autoclave result in parts with high fibre-volume content and low voids [1]. The curing cycle typically begins with the heat-up period when the laminate stack is heated to a predetermined curing temperature. Once cure temperature is attained, the dwelling time begins with the cure temperature being maintained for a given duration, allowing enough time for the individual laminate plies to consolidate into one final part. After curing, the part is cooled down, debagged, and taken out for finishing processes [2].

Despite its benefits, autoclave curing is considered one of the most energy consuming curing processes of CFRP manufacturing [3]. This is due to the mode of heat transfer and long duration of the process cycle. Typical autoclave curing occur via forced convection between flowing hot gas under pressure and the bag-laminate-tool element [4]. In the autoclave, air or inert gas, which is usually nitrogen, is heated up via a heating element and circulated in the autoclave via a fan. Energy is required to heat up the inert gas with a pressure up to 10 [bar] (depending on the pressure cycle). Energy is also required to compensate for heat flow to the bag-laminate-tool element, some parts of the autoclave body and heat loss through the autoclave walls.

The high energy consumption of the autoclave during cure is a major contributor to the environmental footprint of manufacturing

* Corresponding author.
E-mail addresses: C.J.Ogugua@tudelft.nl (C.J. Ogugua), s.v.anton@student.tudelft.nl (S.V. Anton), a.p.tripathi@student.tudelft.nl (A.P. Tripathi), m.d.larrabeiti@student.tudelft.nl (M.D. Larrabeiti), s.o.vanhees@student.tudelft.nl (S.O. van Hees), J.Sinke@tudelft.nl (J. Sinke), C.A.Dransfeld@tudelft.nl (C.A. Dransfeld).
[1] https://www.tudelft.nl/staff/c.j.ogugua/?cHash=f954bfd4392df69ca17d64472bf801ff
[2] https://www.tudelft.nl/staff/j.sinke/?cHash=1bada5246e9f7f89f1fa3f75748241bc
[3] https://www.tudelft.nl/staff/c.a.dransfeld/?cHash=e8df6b235ab29e54244d029138f4f601

https://doi.org/10.1016/j.compositesa.2022.107365
Received 13 June 2022; Received in revised form 28 November 2022; Accepted 3 December 2022
Available online 21 December 2022

Nomenclature

$\dot{m}_x$	Gas mass flow in x-axis (kg/s)
$\dot{m}_y$	Gas mass flow in y-axis (kg/s)
$\dot{q}$	Heat flux (W/m^2)
ϵ	Squared internal gas energy constant (J^2/kg)
$\mathbf{e}$	Lattice direction vector (-)
$\mathbf{n}$	Normal unit vector (-)
$\mathbf{R^{eq}}$	Equilibrium relaxation vector (-)
$\mathbf{R}$	Relaxation vector (-)
$\mathbf{x}$	Position vector (m)
$\mathcal{E}$	Emissivity (-)
$\mathcal{M}$	Molar mass (kg/kmol)
$\mathcal{R}$	Radius of numerical domain (m)
μ_A	Ambient air dynamic Viscosity (Pa s)
μ_G	Autoclave gas dynamic Viscosity (Pa s)
ν_{xx}	Diagonal viscous tensor component (m^2/s)
ν_{xy}	Off-diagonal viscous tensor component (m^2/s)
ρ	Mass density (kg/m^3)
σ	Stefan–Boltzmann constant (J/sm^2 K^4)
σ_y	Yield stress (MPa)
τ	Gas relaxation time (-)
A_{wall}	Autoclave surface area (m^2)
C_p	Specific heat (J/kg K)
C_{p_A}	Autoclave body averaged specific heat (J/kg K)
C_{p_B}	Mould assembly breather specific heat (J/kg K)
$C_{p_{CFRP}}$	CFRP panel averaged specific heat (J/kg K)
$C_{p_{Gas}}$	Autoclave enclosed gas specific heat (J/kg K)
$C_{p_{tool}}$	Mould assembly tool plate specific heat (J/kg K)
D_A	Autoclave inner cavity diameter (m)
e	Specific internal gas energy (J/kg)
E_{cycle}	Energy consumed by autoclave cure cycle (J)
f	Microscopic specific velocity of gas molecules (kg/m^2 s)
h	Heat transfer coefficient (W/m^2 K)
h_A	Ambient air heat transfer coefficient (W/m^2 K)
h_G	Autoclave gas heat transfer coefficient (W/m^2 K)
k	Thermal conductivity (W/m K)
M	Mass (kg)
M_A	Autoclave body mass (kg)
M_B	Breather mass (kg)
M_{CFRP}	CFRP panel mass (kg)
M_{tool}	Tool plate mass (kg)
Nu	Nusselt number (-)
p_{cycle}	Autoclave cure cycle maximum pressure (Pa)
p_{Gas}	Autoclave cycle-averaged gas pressure (Pa)
Pr	Prandtl number (m^2/s)
Q	Heat (J)
Q_A	Heat transferred to the autoclave body (J)
Q_M	Heat transferred to the mould assembly (J)
q_{2D}	Two-dimensional heat (J/m)
Q_{3D}	Three-dimensional heat (J)
Q_{Gas}	Heat transferred to the autoclave enclosed gas (J)
Q_{Loss}	Heat lost to the environment (J)
Ra	Rayleigh number (-)
s	Thickness (m)
SF	Safety factor (-)
T	Temperature (K)
t	Time (s)
T_A	Ambient temperature far from the autoclave (K)
T_G	Autoclave gas average temperature (K)
T_{avg}	Average temperature of autoclave wall (K)
T_{W1}	Average temperature on the inner surface of the autoclave (K)
T_{W2}	Average temperature at the surface between the steel and insulation layers (K)
T_{W3}	Average temperature on the outer surface of the autoclave (K)
u_x	X-axis component of the macroscopic gas velocity (m/s)
u_y	Y-axis component of the macroscopic gas velocity (m/s)
v_{Gas}	Autoclave gas fan velocity (m/s)
V_{in}	Autoclave inner volume (m^3)
w	Width of numerical domain (m)

composites parts [3]. A way to tackle this, is to have a better understanding of the energy usage during an autoclave curing process by first quantifying the total energy consumed by an autoclave and then breaking it down into energy consumed by each heat absorbing elements within the autoclave. For instance, energy that goes to the laminate stack, the flowing gas, the autoclave body and heat lost through the autoclave wall. This would help provide insight on energy intensive areas to focus on for possible improvement.

According to Seow et al. [5] improved monitoring and control of energy used in manufacturing facilities, play a vital role in reducing energy consumption of manufacturing processes. Most research on determining energy consumption of the autoclave process have been directed towards creating an energy inventory for cost estimation or in life cycle assessment (LCA) studies These studies have estimated energy consumption either by direct measurement using power meters [3,6] or by multiplying the power capacity of the autoclave with the processing time [7]. Although direct measurements of autoclave consumption provide an accurate energy demand of the autoclave, it has some limitations. Suitable equipment-specific power meters are not yet readily installed in all commercial architecture. Also, obtained results are specific to the cure cycle monitored and may not be transferable to different cure cycles and process parameters. On the other hand, estimating energy consumption by multiplying the power capacity of autoclave with curing time is certainly an assumption as it neglects the variation in energy demand during heating, dwell or curing stages. In addition to these limitations, these two methods do not provide a breakdown of energy consumption during cure, to account for energy going to the different components of the autoclave including energy consumption due to heat loss through the autoclave walls or heat transfer to the autoclave structural body. Hence, they may not be useful in improving energy efficiency of the autoclave curing process.

The energy consumption of an autoclave is directly connected to the heat flow occurring between the autoclave, the CFRP part to be cured, and the external surrounding. Current methods of modelling autoclave heat transfer processes involve transient turbulent flow simulations of the enclosed gas of the autoclave around a detailed 3D model of its structure. In most studies [8–10], an incompressible Reynolds-Averaged Navier Stokes (RANS) formulation coupled with a k-ϵ turbulence model and a wall function is used. The k-ϵ model is chosen as it allows for a coarse mesh to be used. However, Bohne et al. [11] and Zhao et al. [12] obtained results with the Spalart–Allmaras turbulence model using the commercial computational fluid dynamics (CFD) solver ABAQUS CFD [11,13]. The methods outlined in these studies, while reliable, require a detailed knowledge of the autoclave design and operational procedure and may also require the use of expensive commercial CFD solvers. This makes this approach less suitable for cases where the design information is incomplete or software unavailable. This is common in LCA studies and energy cost evaluations within the aerospace industry, as most data required to perform these studies in the industry are proprietary and not readily available [14]. Hence, novel approaches are necessary to perform such predictions with scarcity of process and design data.

The aims of this paper are: First to present simpler but accurate models for estimating the energy consumption of an autoclave during cure and attribute the estimated energy flows to different elements within the autoclave. Second is to perform a what-if analysis that shows how the autoclaves energy consumption varies with changes in process parameters.

2. Methodology

2.1. Theoretical background

Energy modelling for an autoclave cure cycle is directly linked to the heat flows through each of its main components, and the heat lost to the external environment. The principal processes driving these flows are thermal convection and diffusion. The effects of thermal radiation have been considered negligible in previous studies on the temperature distribution within autoclaves [4,15,16]. However, the study by Kluge et al. [17] shows that thermal radiation is a heat transfer mechanism that occurs in autoclaves and should be considered, although its effect is less significant than convection and conduction. Another source of energy to be considered is the heat produced by the exothermic reaction of the epoxy resin during curing. Its effect on the overall energy consumption was considered negligible in this study due to two reasons. First, the total reaction heat for epoxy resins ranges between 0.12–0.6 [kJ/g] [18,19]. Considering that the epoxy resin composition of our case study CFRP panel is 205 g, The total heat of reaction would range between 0.00683–0.0342 [kWh]. This number is significantly small in comparison to the overall energy consumption of autoclave curing. Secondly, studies by Xie et al. [20] and Dong et al. [21] also show that the curing reactions raise the heat of the mould configuration, on average, by 10 to 15 [°C] above the preset temperature of the cycle for short periods of time. Hence, their effects on the total energy consumed is negligible.

To obtain an estimation of the energy consumed for a preset cure cycle, the first two phenomena have to be modelled in the solid autoclave body as well as in the enclosed gas within it. This study proposes two methodologies for modelling these heat transfer phenomena and subsequently the energy consumption of an autoclave during curing. The first method presented in Section 2.3 is an analytical method based on fundamental thermodynamics equations. This method assumes the energy consumed per cycle is composed of the heat transferred to the autoclave body, mould configuration and enclosed gas, as well as the heat lost to the surrounding environment. The heat transfers are computed using basic thermodynamic equations based on average temperature values in the aforementioned elements. Thermal radiation and the exothermic heat produced by curing are not modelled in this method.

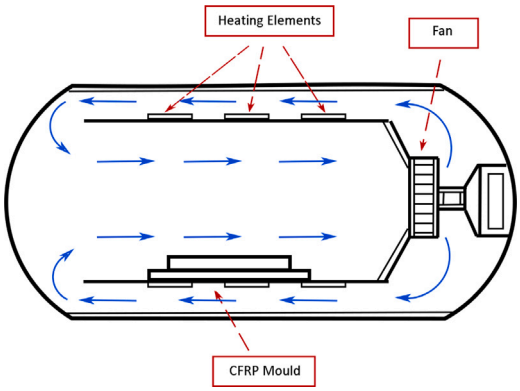

Fig. 1. Sketch of the longitudinal cross-section of the TU Delft laboratory-scaled autoclave. The blue arrows represent the direction of the gas flow during curing.

The second method, developed in this study, is presented in Section 2.4. This method uses a two-dimensional (2D) Multi-Relaxation-Time Lattice Boltzmann method (MRT LBM), based on Yang et al. [22] to simulate the transient autoclave gas velocity and temperature flows. This is combined with a 2D Fourier Heat Equation, which estimates the heat flows through the solid bodies and solid–fluid boundaries. The heat transfer due to thermal radiation was also taken into account for this method. This was done using the Stefan–Boltzmann law of radiation. However, the exothermic heat produced by the curing process is still neglected. A python code implementation of this model was generated for this paper, and is available as supplementary material on the internet hosting service and version control "GitHub", and archived in the general-purpose repository, Zenodo [23].

2.2. Case study autoclave cycle

Autoclaves used for curing composites are cylindrical pressure vessels and come in various sizes. Modelling the heat flows in an autoclave require an understanding of its main components and their heat transfer mechanism. To model heat flows within an autoclave during curing, Antonucci et al. [4] simplified the autoclave components into the autoclave body, a mould assembly and circulating gas.

In this study, an autoclave cycle was selected to help identify the various components within it that can influence heat flows and subsequently its energy consumption. This case study cycle was also used to generate inputs that were applied to the developed models as shown in Section 2.4.7 and for validation of the models as shown in Section 3.3. The autoclave Scholtz (LF7M03) owned by the faculty of Aerospace Engineering, Delft University of Technology, was selected as the case study autoclave. It has a maximum loading panel size of 1.08 [m] × 1.70 [m] and volume of 4.5 [m^3]. The autoclave body consists of a load-bearing steel structure, an insulation layer, heating elements and a fan as shown in Fig. 1.

A cure cycle for thermoset composites typically consists of a temperature and a pressure cycle. The temperature cycle begins with the introduction of heat, which initiates the cross-linking of the polymer matrix. Initial application of heat also leads to reduction in resin viscosity, allowing it to flow and saturate the fibre reinforcements. Once cure temperature is reached, the dwelling stage begins, where temperature is maintained for a period of time. At this stage, the resin viscosity begins to increase until cross-linking is completed. Pressure is applied during the cure cycle to foster removal of trapped air in the composite part, and to enhance part consolidation [24,25]. Cure cycles for polymer matrix systems are usually developed empirically, hence a matrix system may have several cure cycles, with each cure cycle

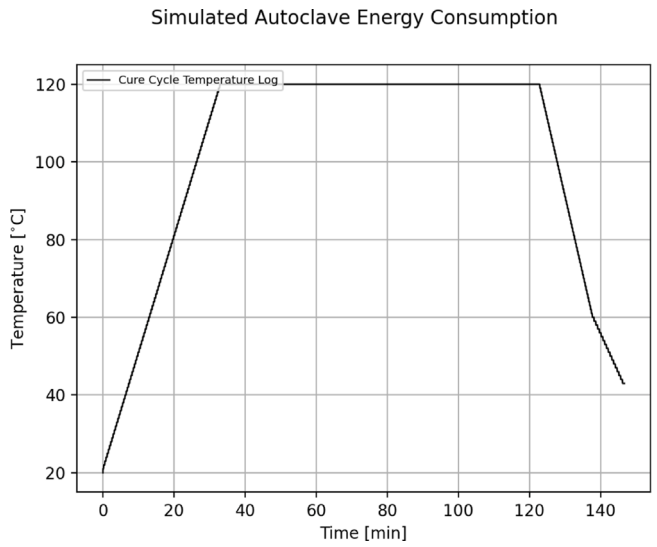

Fig. 2. Preset temperature log of the cycle used for the curing of a CFRP panel in the TU Delft autoclave.

leading to an optimized property in the cured part or accounting for laminate thickness [24].

The CFRP panel considered in this study is made from a carbon fibre (CF)/epoxy prepreg "Deltatech GG200T - DT120" using a standard cure cycle "1.5 h @ 120 [°C]", which is a recommended cycle in the prepreg manufacturer datasheet. This panel was cured in a mould assembly consisting of an aluminium tool plate and breather materials. The circulated gas in this cycle was Nitrogen gas. A summary of the data from the case study autoclave cycle that served as inputs to the proposed models is shown in Table 1.

2.3. Analytical energy consumption model

This section covers the analytical procedure for estimating the energy consumed by autoclaves running CFRP cure cycles. It is based on fundamental thermodynamics laws, combined with existing empirical models for estimating the heat loss through the autoclave walls during a cycle. The procedure makes use of the following properties of the autoclave, CFRP part and mould configuration, and cure cycle.

- autoclave mass $\mathbf{M_A}$ [kg];
- autoclave specific heat $\mathbf{C_{P_A}}$ [J/kgK];
- autoclave inner volume $\mathbf{V_{in}}$ [m^3];
- autoclave gas type and pressure $\mathbf{p_{Gas}}$ [bar];
- autoclave gas specific heat $\mathbf{C_{P_{Gas}}}$ [bar];
- autoclave wall surface area $\mathbf{A_{wall}}$ [m^2];
- autoclave wall layer thicknesses: $\mathbf{t_1}$, $\mathbf{t_2}$, ..., $\mathbf{t_n}$
- autoclave wall layer conductivities: $\mathbf{k_1}$, $\mathbf{k_2}$, ..., $\mathbf{k_n}$.

Similarly, for the mould configuration residing in the autoclave, the following parameters are of interest:

- CFRP mass $\mathbf{M_{CFRP}}$, [kg];
- CFRP specific heat $\mathbf{C_{P_{CFRP}}}$ [J/kgK];
- tool plate mass $\mathbf{M_{Tool}}$ [kg];
- tool plate specific heat $\mathbf{C_{P_{Tool}}}$ [J/kgK];
- breather mass $\mathbf{M_B}$ [kg];
- breather specific heat $\mathbf{C_{P_B}}$ [J/kgK],

The cure cycle is approximated with a linear interpolation between a series of known temperature points:

$$(t_0, T_0) \longrightarrow (t_1, T_1) \longrightarrow \ldots \longrightarrow (t_n, T_n) \longrightarrow (t_0, T_0)$$

Table 1
Summary of the collected data about the autoclave and CFRP panel used for the curing process.

Data collected	Values and units	Measurement error
Autoclave Mass	1102 kg	<< 1 %
Autoclave Outer Length	3.4 m	<< 1 %
Autoclave Inner Length	3 m	<< 1 %
Autoclave Outer Diameter	1.55 m	<< 1 %
Autoclave Inner Diameter	1.25 m	<< 1 %
Autoclave Total Volume	6.2 m^3	<< 1 %
Autoclave Inner Volume	4.5 m^3	<< 1 %
Autoclave Surface Area	13.84 m^2	<< 1 %
Autoclave Specific Heat Capacity	513.6 J/kg K	10%
Autoclave Thermal Conductivity	1.2 W/mK	10%
Autoclave Wall Thickness	0.14 m	<< 1 %
CFRP Panel Dimensions	0.45 × 0.45 × 0.012 m	<< 1 %
CFRP Number of Layers	12 –	–
Fibre Mass	0.48 kg	<< 1 %
Fibre Specific Heat	750 J/kg K	10%
Fibre Thermal Conductivity	171 W/mK	10%
Resin Mass	0.205 kg	<< 1 %
Resin Specific Heat	1850 J/kg K	10%
Resin Thermal Conductivity	0.1 W/mK	10%
Bleeder Mass	0.242 kg	<< 1 %
Bleeder Specific Heat	1350 J/kg K	10%
Bleeder Thermal Conductivity	0.5 W/mK	10%
Bleeder Dimensions	0.7 × 0.7 × 0.00025 m	<< 1 %
Tool Plate Mass	12.15 kg	<< 1 %
Tool Plate Dimensions	0.8 × 0.8 × 0.009 m	<< 1 %
Tool Plate Specific Heat	921 J/kg K	10%
Tool Plate Thermal Conductivity	200 W/mK	10%
Gas Type	Nitrogen	–
Gas Viscosity	$1.81 \cdot 10^{-5}$ Pa s	10%
Gas Specific Heat	1040 J/kg K	10%
Gas Thermal Conductivity	0.04 W/mK	10%
Fan Speed	6 m/s	<< 1 %
Ambient Air Temperature	20 °C	<< 1 %
Ambient Air Density	1.225 kg m^3	<< 1 %
Ambient Air Viscosity	$1.81 \cdot 10^{-5}$ Pa s	<< 1 %

Table 2
Summary of the input parameters used for the MRT LBM simulation of the TU Delft autoclave gas flow.

Simulation parameters	Values and units
Spatial Discretization Step	0.013 m
Time Discretization Step	0.013 s
2D Domain Length	4.3 m
2D Domain Width	1.65 m
Heating Element Temp.	190 K
Autoclave Outer Length	3.4 m
Autoclave Inner Length	3 m
Autoclave Outer Diameter	1.55 m
Autoclave Inner Diameter	1.25 m
Autoclave Thermal Conductivity	0.8 - 1.2 W/mK
2D Mould Dimensions	0.45 × 0.0012 m
Gas Viscosity	$1.81 \cdot 10^{-5}$ Pa· s
Gas Specific Heat	1040 J/kgK
Gas Thermal Conductivity	0.04 W/mK
Fan Speed	6 m/s
Ambient Air Temperature	20 °C
Ambient Air Density	1.225 kg m^3
Ambient Air Viscosity	$1.81 \cdot 10^{-5}$ Pa· s

where t_i [s] and T_i [K] are the times and temperatures at instances i in the cure cycle. These instances are linearly interpolated to obtain a continuous function $T(t)$, as shown in Fig. 3.

The model considers the total energy consumption of the autoclave for this cure cycle to be composed of the heat flow to the autoclave body, Q_A [J], the heat flow to the gas Q_{Gas} [J], the heat flow to the CFRP mould, Q_M [J] and the heat lost through the walls to the surrounding environment Q_{Loss} [J]:

$$E_{cycle} = Q_A + Q_M + Q_{Gas} + Q_{Loss} \quad (1)$$

This equation only takes into account the significant contributions to the energy consumption of the cycle, for the sake of simplicity. The effect of exothermic curing reaction on energy consumption is considered negligible due to the reasons explained in the beginning of Section 2.1. Thermal radiation is also not considered in this method for two reasons. First, heat transfer due to thermal radiation in an autoclave is considered small and negligible in a number of studies [4,15]. Secondly, estimating the heat loss due to thermal radiation requires a more precise prediction of the average surface temperature of the autoclave. Thermal radiation of an object surrounded by air, according to Zhang et al. [26], is given by Eq. (2):

$$\frac{dQ}{dt} = \sigma \mathcal{E} A \left(T_{W3}^4 - T_A^4\right) \tag{2}$$

where $\frac{dQ}{dt}$ is the heat time rate [W], $\sigma = 5.67 \cdot 10^{-8}$ [J/s m^2 K^4] is the Stefan–Boltzmann constant, $\mathcal{E}$ is the emissivity of the object material [-], A is its surface area [m^2] T_{W3} is its surface temperature [K] and T_A is the air temperature away from the object. If $T_{W3} \approx T_A$, then $\frac{dQ}{dt} \approx 0$. As seen in the equation above, the 4th power in the temperature term makes it a sensitive parameter when estimating heat loss due to thermal radiation. For an ambient temperature of 20 [°C], a surface temperature of 25 [°C] and an emissivity of 0.3, an overestimation of 10 [°C] in the surface temperature would increase the radiation flux from 9 W/m^2 to 28 W/m^2. This is a 300% increase which would add to the error in estimating energy consumption. The analytical method does not take into consideration the temperature variations at the walls of the autoclave. This simplification may lead to an overestimation of the heat loss due to radiation as well as the total energy consumption. **The body heat flows** (Q_A, Q_M **and** Q_{Gas}) depend solely on the initial and maximum values of the temperature in the cure cycle, and can be modelled using Eq. (3):

$$Q = M \cdot C_P \cdot \Delta T \tag{3}$$

where M is the mass [kg], C_P is the specific heat [J/kg K] and ΔT is the temperature difference [K].

This equation is used only for positive or neutral temperature gradients, as the energy required for cooling is provided by a separate system. Thus, **the mould assembly heat flow** is given by Eq. (4):

$$Q_M(t) = (M_{CFRP} \cdot C_{P_{CFRP}} + M_{Tool} \cdot C_{P_{Tool}} + M_B \cdot C_{P_B}) \cdot (T(t) - T_A), \quad \frac{\partial T}{\partial t}(t) \geq 0 \tag{4}$$

where $T(t)$ is the continuous cure cycle temperature [K]. The cycle temperature at time t [s] is taken when $\frac{\partial T}{\partial t} \geq 0$, to exclude the cooling energy consumption from the equation. Similarly, **the gas heat flow** is given by Eq. (5):

$$\begin{aligned} Q_{Gas}(t) &= M_{gas} \cdot C_{P_{Gas}} \cdot (max(T(t)) - T_A) \\ &= \frac{P_{Gas} \cdot V_{in} \cdot \mathcal{M}_{Gas}}{R \cdot T_A} \cdot C_{P_{Gas}} \cdot (max(T(t)) - T_A) \end{aligned} \tag{5}$$

where $\mathcal{M}_{Gas}$ is the gas molar mass [g/mol K].

The wall heat loss (Q_{Loss}) is computed based on Fourier law, assuming a convective heat flow with the surrounding gas/air. Fig. 4 shows a hypothetical temperature variation through said wall.

With an assumed $\dot{q}$, it is possible to calculate the temperature drops between the different layers. For instance, as the heat flows from the inside of the autoclave to the wall, it sees a decrease in temperature from T_0 to T_1, quantified in part by the heat transfer coefficient of the autoclave gas, h_G, as in Eq. (6):

$$T_{W1} = T_G - \frac{\dot{q}}{h_G} \tag{6}$$

where A_{wall} is the surface area of the autoclave walls, and the heat transfer coefficient, h_G is approximated with the semi-empirical Dittus/Boelter Equation for forced convection inside a cylindrical wall [27]:

$$h_G = 0.023 \frac{k}{D_A} \left(\frac{\rho V_{Gas} D_A}{\mu}\right)^{0.8} \cdot \left(\frac{\mu_G C_{P_{Gas}}}{k}\right)^{0.4} \tag{7}$$

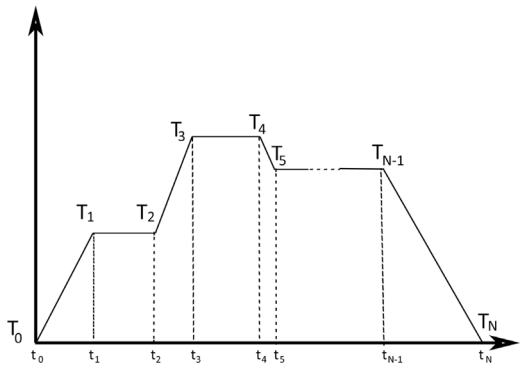

Fig. 3. Sketch of a linear temperature log, programmed in autoclave CFRP cure cycles. The x-axis represents time, while the y-axis represents temperature.

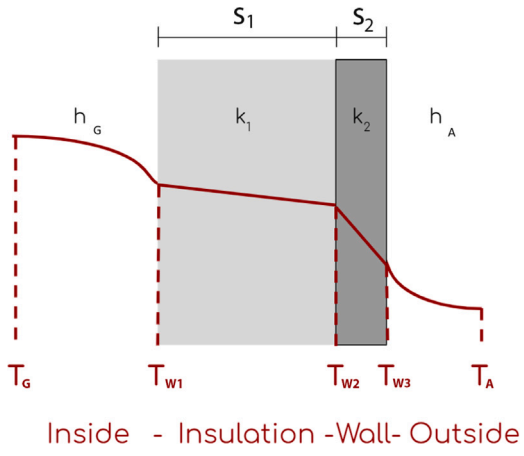

Fig. 4. Schematic of the heat flow through the autoclave wall. Temperature ranges from T_G (inside the autoclave), to T_A (outside the autoclave). It shows the thickness and thermal conductivity of the insulator (W1) and the steel wall (W2), and the convective heat transfer coefficients of the nitrogen gas (G) and the outside air (A).

In the equation above, μ_G is the dynamic viscosity of the gas [kg/ms] and V_{Gas} is its velocity [m/s]. D_A represents the inner diameter of the autoclave [m], and ρ is the density of the gas [kg/m^3].

In contrast, the temperature decrease through **one layer of the wall** depends on the wall thickness s_i and its thermal conductivity k_i. This applies to both the insulating and steel layer and is given by Eq. (8):

$$T_{i+1} = T_i - \dot{q} \frac{s_i}{k_i} \tag{8}$$

Finally, the temperature difference from T_{W3} to T_A is given by Eq. (9):

$$T_A = T_{W3} - \frac{\dot{q}}{h_A} \tag{9}$$

where h_A is the air natural convection heat transfer coefficient, approximated using the empirical law found by Incropera for free convection around a horizontal cylinder [28], given by Eq. (10):

$$h_A = \frac{N_u \cdot k_a}{D_A}, \quad N_u = \left(0.60 + \left(\frac{0.387 \cdot R_a^{\frac{1}{6}}}{\left(1 + \left(0.0559 P_r^{-1}\right)^{\frac{9}{16}}\right)^{\frac{8}{27}}}\right)\right)^2,$$
$$P_r = \frac{C_{P_{Air}} k_a}{D_A}, \quad R_a = P_r \cdot \frac{g \beta D_A^3 \rho_a^2 \left(T_{W3} - T_A\right)}{\mu_a^2} \tag{10}$$

Here, N_u [-], P_r [m^2 s^{-1}], and R_a [-], are the Nusselt, Prandtl, and Rayleigh numbers; that describe the convective behaviour of the gas.

β is the coefficient of volume expansion, usually equal to $\beta = 0.0034$ $[1/K]$, and g is the gravitational acceleration $[m/s^2]$.

With the value of h_A, $\dot{q}$ can be recalculated iteratively using the temperature difference between the inside and the outside of the autoclave (T_G and T_A), resulting in Eq. (11)

$$\dot{q} = \frac{T_G - T_A}{\frac{1}{h_A} + \frac{s_1}{k_1} + \frac{s_2}{k_2} + \frac{1}{h_G}} \tag{11}$$

Once the heat flow value for the cure temperature is calculated, the heat flow value for other temperatures within the cure cycle can then be calculated as this simple model is linear, and so $\frac{\dot{q}}{\Delta T} = \text{constant}$. Once the heat flow is calculated for every point of interest, the heat loss, Q_{Loss} of the autoclave, is the result of Eq. (12).

$$Q_{Loss} = A_{wall} \int_0^t \dot{q}(t)dt \tag{12}$$

Finally, **the heat flow to the autoclave body** is defined in part through the partial steps of the heat loss model. As the autoclave wall will experience different temperatures, it is useful to define a temperature that represents the weighted average of the different layers of the autoclave. Just like the gas and mould heat flows, the reference temperature will be the maximum temperature until time t. In this case, this is the temperature that will be used to calculate the rest. Then, if T_{W1}, T_{W2}, T_{W3} are the temperatures at the inner, middle, and outer sections of the wall, respectively, the weighted averaged temperature T_{avg} is then defined through Eq. (13).

$$T_{avg}(t) = \frac{T_{W1}(t) - T_{W2}(t)}{2} \frac{s_1}{s_1 + s_2} + \frac{T_{W2}(t) - T_{W3}(t)}{2} \frac{s_2}{s_1 + s_2} \tag{13}$$

With the averaged temperature, the heat flow to the autoclave body can be calculated as in Eq. (14).

$$Q_A = M_A \cdot C_{P_A} \cdot (T_{avg}(t) - T_A) \tag{14}$$

To generate an energy consumption variation plot using the analytical method proposed in Section 2.3, this was translated into a computer algorithm written in Python 3.8, with the help of the NumPy and Matplotlib libraries [29,30]. Within this algorithm, the procedure explained above has been applied for a finite set of discretized time steps in the duration of the cure cycle. The properties of the autoclave and mould configuration outlined in Table 1 were used as input parameters for the model, together with the temperature log in Fig. 4.

2.4. Lattice-Boltzmann-based numerical energy consumption model

The analytical model outlined in Section 2.3 provides a first-order estimation of the energy consumed by an autoclave, with little knowledge about the autoclave dimensions, besides its inner diameter, D_A. For more accurate predictions, however, a more detailed analysis is required. The model presented in this section utilizes general geometrical parameters of autoclaves and CFRP mould assemblies, and by making use of the axis of symmetry typically found in autoclave designs, performs a 2D analysis of the heat transfers occurring during a cure cycle for a given temperature log. The novelty in the procedure lies in MRT LBM simulation of the gas flow inside the autoclave, with a solid heat simulation of the autoclave body itself and the mould assembly within it. The coupling is performed using convective boundary conditions, based on empirically-determined heat transfer coefficients. The purpose of the MRT LBM simulation, besides estimating the convection and diffusion of the autoclave gas, is to calculate its temperature at the inner surface of the autoclave walls. This temperature distribution is necessary in the determination of the heat loss to the surrounding environment, through the autoclave walls. As this model accounts for temperature variations within the autoclave components, it is expected to yield more accurate results, compared to the analytical method presented in Section 2.3. However, similar to that method, this model neglects the heat produced by the exothermic curing reaction of the CFRP panel.

2.4.1. Multi-relaxation-time Lattice-Boltzmann flow modelling

This subsection covers the theory behind fluid flow modelling, adapted for the specific case of heated autoclave convected gas. As discussed in Torres et al. [31], an autoclave curing cycle involves a variation of temperature and pressure of the enclosed gas within it. This is done to achieve a desired curing sequence for a CFRP part. Therefore, to perform a CFD simulation of the entire cycle, one would require a compressible solver to account for the pressure variation. Such simulations over the duration of an entire cure cycle are often impractical, as they consume computational time and resources. As a result, many CFD studies on autoclaves are performed over a short period of the time in the curing cycle, such as [8,10,11], after which the results are extrapolated for the entire cycle. Given the short time span, the pressure variation experienced is negligible and the flow is assumed incompressible. A similar approach is adopted in this study, for modelling convective and diffusive heat processes in the autoclave. As pointed in the three scientific papers mentioned above, the gas speeds in an autoclave do not exceed 10 [m/s] throughout a cycle. This leads to Mach numbers in the order of $M \approx 10^{-2}$, which, according to [32], imply incompressible behaviour in the flow. Considering the larger goal of modelling heat transfer and having robustness in mind, an MRT LBM 2D formulation was chosen for solving the transient velocity field of the gas. For this study, the method proposed by Yang was utilized [22], and it is briefly summarized below.

Firstly, the fluid domain is discretized in a series of square cells, with discrete points at the corners. For each corner, 9 microscopic velocities are defined at the centre and each cardinal point: $\mathbf{e_0} = [0,0]$, $\mathbf{e_N} = [0,1]$, $\mathbf{e_S} = [0,-1]$, $\mathbf{e_E} = [1,0]$, $\mathbf{e_W} = [-1,0]$, $\mathbf{e_{NE}} = [1,1]$, $\mathbf{e_{NW}} = [-1,1]$, $\mathbf{e_{SE}} = [1,-1]$, $\mathbf{e_{SW}} = [-1,-1]$. These velocities represent the statistical average speed of the gas molecules in a specific orientation. For each velocity, a particle distribution function matrix $\mathbf{F^t} = [f_0, f_N, f_S, f_E, f_W, f_{NE}, f_{NW}, f_{SE}, f_{SW}]^T$ is defined at time t with f_i being the fraction of fluid particles travelling in direction i. The fluid domain is shown in Fig. 5.

At the root of this method, lies the Boltzmann Transport Eq. [33] shown in Eq. (15):

$$\frac{\partial f_i}{\partial t} + \mathbf{e_i} \cdot \nabla f_i = \Omega_i \tag{15}$$

This equation describes the change in time of every microscopic velocity in the method and can be discretized using forward differentiation, which yields:

$$f_i\left(\mathbf{x} + \mathbf{e_i}\partial t, t + \partial t\right) = f_i(\mathbf{x}, t) - \frac{1}{\tau}\left(f_i(\mathbf{x}, t) - f_i^{eq}(\mathbf{x}, t)\right) \tag{16}$$

where τ is the dimensionless relaxation time towards equilibrium, $\mathbf{x} = [x, y]^T$ is the position vector in Cartesian coordinates and $f_i^{eq}(\mathbf{x}, t)$ is the equilibrium state of the distribution function f_i according to the Boltzmann distribution [22]. This equation is split into two steps for each time interval: the collision step and the streaming step.

The collision step consists of redistributing, for every cell, the incoming microscopic velocities f_i, according to the Boltzmann Distribution [33]. Firstly, the macroscopic parameters of the flow are computed using the microscopic velocities f_i. This is done in a matrix–vector form, in Eq. (17), as shown in [22].

$$\mathrm{R} = \begin{bmatrix} \rho \\ e \\ \epsilon \\ m_x \\ q_x \\ m_y \\ q_y \\ v_{xx} \\ v_{xy} \end{bmatrix} = \begin{bmatrix} 1 & 1 & 1 & 1 & 1 & 1 & 1 & 1 & 1 \\ -4 & -1 & -1 & -1 & -1 & 2 & 2 & 2 & 2 \\ 4 & -2 & -2 & -2 & -2 & 1 & 1 & 1 & 1 \\ 0 & 1 & -1 & 0 & 0 & 1 & -1 & -1 & 1 \\ 0 & -2 & 2 & 0 & 0 & 1 & -1 & -1 & 1 \\ 0 & 0 & 0 & 1 & -1 & 1 & -1 & 1 & -1 \\ 0 & 0 & 0 & -2 & 2 & 1 & -1 & 1 & -1 \\ 0 & 1 & 1 & -1 & -1 & 0 & 0 & 0 & 0 \\ 0 & 0 & 0 & 0 & 0 & 1 & 1 & -1 & -1 \end{bmatrix} \cdot \begin{bmatrix} f_0 \\ f_N \\ f_S \\ f_E \\ f_W \\ f_{NE} \\ f_{NW} \\ f_{SE} \\ f_{SW} \end{bmatrix} \tag{17}$$

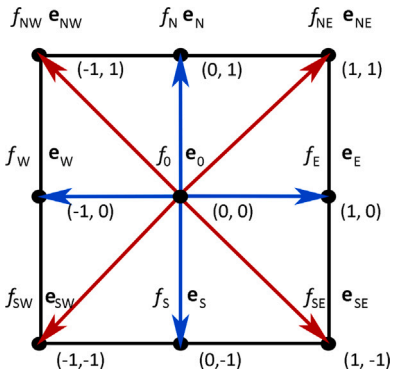

Fig. 5. Sketch of the fluid domain for the MRT LBM, showing the coordinates of the microscopic velocities and their corresponding distribution functions.

where **R** is the relaxation vector, and it is computed from the microscopic velocity vector, **F**. Rewritten in a shorter form for a specific time step, Eq. 17 becomes:

$$\mathbf{R}^n = \mathbf{M} \cdot \mathbf{F}^n, \tag{18}$$

Where n is the index of the time frame. Next, the macroscopic parameters of the relaxation vector are partially redistributed in time to their equilibrium state, using a relaxation matrix **S** and the equilibrium state vector $\mathbf{R}^{\mathbf{eq}}$ described by Yang et al. [22], with Eq. (19).

$$\mathbf{R}^{\mathbf{n}+\frac{\mathbf{1}}{\mathbf{2}}} = \mathbf{R}^{\mathbf{n}} - \mathbf{S} \cdot \left(\mathbf{R}^{\mathbf{n}} - \mathbf{R}^{\mathbf{eq}}\right) \tag{19}$$

The matrix **S** has been defined by Yang et al. [22] empirically. The algorithm is found to perform best by using the following values:

$$\mathbf{S} = \left[0 \quad 1.1 \quad 1.3 \quad 0 \quad 1.8 \quad 0 \quad 1.8 \quad \frac{1}{\tau} \quad \frac{1}{\tau}\right] \cdot \mathbf{I} \tag{20}$$

where **I** is the identity matrix. According to Yang et al. [22], the equilibrium $\mathbf{R}^{\mathbf{eq}}$ matrix is given by Eq. (21):

$$\mathbf{R}^{\mathbf{eq}} = \left[\rho \quad -2\rho + 3 \cdot \left(u_x^2 + u_y^2\right) \quad \rho + 3 \cdot \left(u_x^2 + u_y^2\right) \quad 0 \quad -u_x \quad 0 \quad -u_y \quad u_x^2 - u_y^2 \quad u_x \cdot u_y\right]^T \tag{21}$$

where $u_x = \frac{1}{\rho}\left(f_E + f_{NE} + f_{SE} - f_W - f_{NW} - f_{SW}\right)$ and $u_y = \frac{1}{\rho}\left(f_N + f_{NE} + f_{NW} - f_S - f_{SW} - f_{SE}\right)$ are the macroscopic velocities (m/s). Using these two matrices, the new distribution functions after the collision step can be computed with Eq. (22):

$$\mathbf{F}^{\mathbf{n}+\frac{\mathbf{1}}{\mathbf{2}}} = \mathbf{M}^{-\mathbf{1}} \cdot \mathbf{R}^{\mathbf{n}+\frac{\mathbf{1}}{\mathbf{2}}} \tag{22}$$

Next, the streaming step is performed. This step advects the particle distribution functions f_i in $\mathbf{F}^{\mathbf{n}+\frac{\mathbf{1}}{\mathbf{2}}}$ between the cells of the domain. To simplify calculations, the MRT-LBM requires $\partial x = \partial t$. The streaming equation is simply:

$$f_i^{n+1}\left(x + e_i \partial t, t + \partial t\right) = f_i^{n+\frac{1}{2}}\left(x, t + \partial t\right) \tag{23}$$

This concludes the algorithm for one time step. The same procedure is repeated for every following time step. Solid boundary conditions are handled by the impulse method, as shown in [33]. This method assumes the flow particles to experience perfectly-elastic collisions with the walls of the solid boundaries, and thus, return to their opposite direction with a velocity equal in magnitude.

2.4.2. Gas heat flow modelling

Approximating the heat flow through the autoclave gas requires the modelling of two phenomena mentioned in the beginning of Section 2.3: convection and diffusion. While the latter can be resolved using a Laplacian equation with the initial and boundary conditions for the temperature field [34], the former requires information about the gas velocity in the computational domain. To solve the temperature field, a coupling between the velocity field outputted by the MRT LBM method presented in the previous section and the Laplacian heat equation is proposed, through Eq. (24), taken from White et al. [34]:

$$\frac{\partial T}{\partial t} = \frac{k}{\rho C_p}\nabla^2 T - \vec{u} \cdot \nabla T \tag{24}$$

where $\vec{u}$ is the previously computed velocity field at an arbitrary time. The term on the left accounts for the heat diffusion through the gas, while the term on the right models thermal convection. This equation is discretized in 2D using central and forward difference schemes, as follows in Eq. (25):

$$\begin{aligned} T(x,y)^{n+1} &= T^n(x,y) \\ &+ \Delta t \cdot \left(\frac{k}{\rho C p}\left(\frac{T(x+\Delta x,y) - 2T(x,y) + T(x-\Delta x,y)}{\Delta x^2} + \right.\right. \\ &\left.\left. + \frac{T(x,y+\Delta y) - 2T(x,y) + T(x,y-\Delta y)}{\Delta y^2}\right)\right. \\ &\left. - u_x \cdot \frac{T(x+\Delta x,y) - T(x-\Delta x,y)}{2\Delta x} - u_y \cdot \frac{T(x,y+\Delta y) - T(x,y-\Delta y)}{2\Delta y}\right) \end{aligned} \tag{25}$$

The expression in the parenthesis multiplied with Δt is denoted $g(T,x,y,t)$, and then a 4th order Runge–Kutta scheme is applied to solve for $T(x,y)^{t+1}$, as shown below:

$$k_1 = \Delta t g(T,x,y,t), \quad k_2 = \Delta t g\left(T + \frac{k_1}{2}, x, y, t\right),$$

$$k_3 = \Delta t g\left(T + \frac{k_2}{2}, x, y, t\right), \quad k_4 = \Delta t g\left(T + k_3, x, y, t\right)$$

$$T^{n+1} = T^n + \frac{1}{6}\left(k_1 + 2 \cdot k_2 + 2 \cdot k_3 + k_4\right). \tag{26}$$

This system is posed uniquely, using proper boundary and initial conditions. At the edges of the heating elements, the temperature is kept to the one dictated by the cure cycle, using a Dirichlet boundary condition. At the autoclave walls, heat loss is modelled in a simplified way, using the same procedure as described in Section 2.3, with Eq. (12). The heat transfer coefficients in that equation are modelled using the Dittus/Boelter empirical laws (Eq. (7) and (10)) for forced and free convection around a cylinder [27]. This heat flow through the autoclave walls is, however, simulated as described in Section 2.4.3, by means of the Fourier Heat Equation [4]. A section of a generic autoclave wall and its insulator and load-bearing steel layer is depicted in Fig. 4, where the steady-state temperature gradients, as assumed by the analytical model, are also plotted as a function of thickness.

2.4.3. Solid heat flow modelling

For the simulation of heat flow through the solid surfaces, the only thermodynamic phenomenon that must be modelled is heat diffusion [4]. For this model, only the autoclave body and the mould assembly are considered in the solid heat flow simulations. These simulations are done with the Fourier Heat Equation [4], applied to a 2D representation of the autoclave body, which accounts for the load-bearing and insulation layer of the structure. The Fourier Heat Equation is given by Eq. (27), and it is applied with convective boundary conditions:

$$\frac{\partial T}{\partial t} = \frac{k}{\rho C_p}\left(\frac{\partial^2 T}{\partial x^2} + \frac{\partial^2 T}{\partial y^2}\right). \tag{27}$$

This equation is discretized into an algebraic system using central and forward difference schemes, as shown in Eq. (28):

$$\begin{aligned} T(x,y)^{n+1} = T^n(x,y) + \Delta t \cdot \left(\frac{k}{\rho C p}\left(\frac{T(x+\Delta x,y) - 2T(x,y) + T(x-\Delta x,y)}{\Delta x^2}\right.\right. \\ \left.\left. + \frac{T(x,y+\Delta y) - 2T(x,y) + T(xy-\Delta y)}{\Delta y^2}\right)\right. \end{aligned} \tag{28}$$

Similar to the procedure in Section 2.4.2, the expression in the parentheses multiplied with Δt is denoted $g(T, x, y, t)$, and then a 4th order Runge–Kutta scheme is applied to solve for $T(x, y)^{n+1}$, as shown in Eq. (26). The inner and outer walls of the body are modelled with convective boundary conditions, using Eq. (29):

$$\frac{\partial T}{\partial \vec{n}} = h \cdot (T - T_A), \tag{29}$$

where $\vec{n}$ denotes the vector normal to the autoclave's surface. The discretization of this boundary condition is given by Eq. (30):

$$\frac{T(\vec{n} + \vec{\Delta n}) - T(\vec{n})}{\vec{\Delta n}} = h \cdot (T(\vec{n}) - T_A). \tag{30}$$

The heat transfer coefficient (h_G) is determined using the same procedure as in Section 2.3, using Eq. (7).

2.4.4. Thermal radiation heat loss modelling

The final process taken into account by this numerical model is the heat lost to the environment through thermal radiation. While the analytical model proposed in Section 2.3 considers this phenomenon negligible due to its small contribution, it is taken into account here to increase the accuracy of the total heat consumption estimation produced by this one. As shown in Zhang et al. [26], thermal radiation is given by Eq. (31):

$$q_i(t) = \sum_{i=0}^{N_{cells}} \int_0^t \mathcal{E}\sigma\nu A_i \left(T_{W3_i}(\tau)^4 - T_A(\tau)^4 \right) d\tau \tag{31}$$

where $\sigma = 5.67 \cdot 10^{-8}$ [J/s m^2 K^4] denotes the Stefan–Boltzmann constant, A_i is the area of the cells on the outer surface of the autoclave [m^2] and $\mathcal{E}$ is the emissivity of the material in the outer layer of the autoclave.

2.4.5. Total heat consumption calculation

The total energy consumed up to the time instance, $t = n \cdot \Delta t$, where Δt is the time step of the simulation [s], is computed through the summation of all heat transfers occurring in the elements of the simplified autoclave model outlined at the beginning of Section 2.3. The heat 2D flows through the autoclave body, the mould configuration and the enclosed gas are obtained by summing the individual heats of all the cells in the domain, for every time step, with Eq. (32) [35]:

$$q_i^n = q_i^{n-1} + m_i \cdot C_{p_i} \cdot (T_i(t) - T_i(t - \Delta t)) \tag{32}$$

where the heat Q represents either Q_A, Q_M or Q_{Gas}. To obtain the heat lost to the environment until time $t = n \cdot \Delta t$, Eq. (33) is used for the cells at the external edges of the 2D domain in Fig. 8:

$$q_i^n = q_i^{n-1} + \Delta t \cdot h\left(T_i\right) \Delta x \left(T_i(t) - T_A\right) \tag{33}$$

After a conversion from a 2D domain to a 3D domain, the heat components of all elements of the model are summed up, using Eq. (1), which yields an estimation of the total energy in 2D consumed by the autoclave up to a given point in time.

2.4.6. Conversion of model 2D outputs to 3D results

The numerical model proposed in the previous subsections of this section simplifies autoclaves to a 2D domain, and hence, all autoclave model outputs must be converted to 3D properties. This correction is based on the axial symmetry of autoclaves. Therefore, all heat flows occurring in the 2D domain of the autoclave body, namely Q_A and Q_{Loss}, are rotated and integrated along the longitudinal symmetry axis, to obtain volumetric cumulative heats. This is done by means of Eq. (34):

$$Q_{3D} = \int_{\Omega_{2D}} \pi \mathcal{R}(x, y) dq_{2D} \approx \pi \sum_{i=0}^{N_{cells}} \mathcal{R}_i \cdot q_{2D_i} \tag{34}$$

where Ω_{2D} is the 2D domain, Q_{3D} is the total 3D heat flow [kWh], $\mathcal{R}(x, y)$ is the distance between a local point (x, y) in the domain and the axis of symmetry [m], and dq_{2D} is the local heat flow of a differential square element in the 2D domain [kWh/m^3]. The equation uses the term π instead of 2π because the 2D domain must be rotated by an angle of only 180° to describe a full rotational volume.

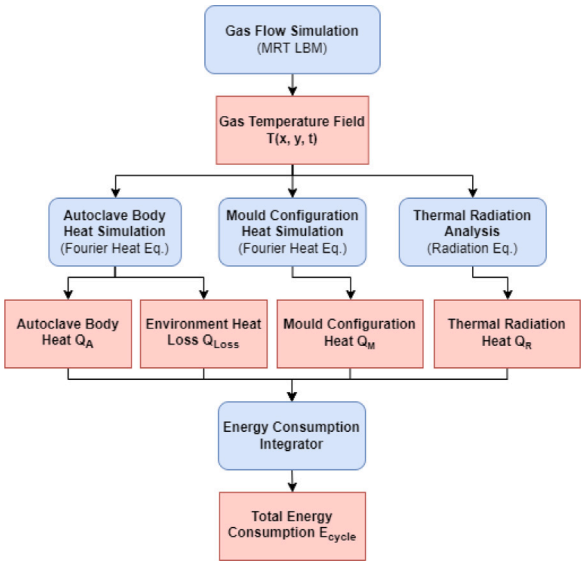

Fig. 6. Program structure for the autoclave energy consumption model. The blue boxes represent sub-algorithms, while the red boxes show intermediary simulated results.

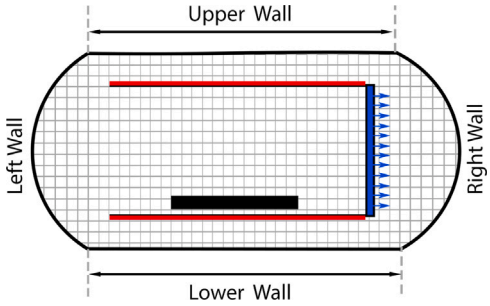

Fig. 7. A sketch of the spatial discretization of the autoclave interior. The blue area has a horizontal velocity set to the fan velocity. The red areas have the temperature set to the heating element temperatures. The black areas are solid, with zero velocity.

Converting the 2D heat flows through the mould configuration with its elements requires a separate procedure. For the CFRP panel, breather and the tool plate, it is assumed that the temperature through the width of the components has a negligible variation. This follows from the study of Bohne et al. [11], where temperature sensors placed on the front and rear of a mould configuration registered a difference below 10 °C. Thus, the 3D heat flow is approximated through Eq. (35):

$$Q_{3D} = \int_{\Omega_{2D}} w(x, y) dq_{2D} \approx \sum_{i=0}^{N_{cells}} w_i \cdot q_{2D_i} \tag{35}$$

where $w(x, y)$ is the width variation of the simplified mould configuration [m], and w_i are the widths of the discretized cells [m].

2.4.7. Algorithmic implementation of the Lattice-Boltzmann model

While Section 2.4.1 to 2.4.6 covered the generalized theory and numerical equations involved in the proposed MRT LBM method, this subsection outlines the computational implementation of these equations for axisymmetric, cylindrical autoclaves used in the curing of CFRP panels. The algorithmic procedure utilized by the model is portrayed in Fig. 6. it begins with the MRT LBM simulation itself, which

produces a steady-state temperature field of the gas within the autoclave. This temperature field is then used to determine the temperature distributions on the inner surface of the autoclave and on the mould configuration. These are then used as boundary conditions for three other heat conduction simulations through the solid structures of the autoclave and mould. The outputs of these simulations are the heat components building up the total energy consumption for a given cycle: the heat transferred to the autoclave body, the heat transferred to the mould configuration, the heat lost to the external environment through convection, and the heat lost through thermal radiation. Finally, these elements are summed together to compute the simulated energy log of the autoclave.

To perform the MRT LBM simulation, a cross-section of the autoclave body is simplified to a 2D collocated Cartesian domain, modelled based on the autoclave geometrical parameters, such as those outlined in Table 1. The internal pressure-vessel shape is maintained through the domain, while the fans and heating elements are modelled regions in the domain where Dirichlet boundary conditions are applied on the velocity and temperature fields. The CFRP mould assembly itself is simplified to a 2D rectangular shape, maintaining its cross-sectional surface area and aspect ratio. A sketch of such a domain is shown in Fig. 7. The solid heat transfer simulations for the autoclave body and mould configuration make use as well of a cross-section of their geometry as a 2D numerical domain. However, the autoclave is represented through a rectangular structure, which simplifies the application of boundary conditions in the domain. It is expected that the effects of this simplification on the resulting energy consumption of a cure cycle to be negligible. This is because the flux of heat through the autoclave walls is independent of their shape, as long as the layer thickness and surface area are preserved. To compute the rectangular shape, besides the wall thickness, the autoclave cross-sectional area has been maintained constant, together with its radius. A similar method is applied to the mould configuration. According to Antonucci et al. [4], the most important components for heat transfer in the mould are the tool plate, the CFRP panel and the bleeder. Therefore, these are considered in the numerical domain. Sketches of such domains are shown in Fig. 8 and Fig. 9. For the autoclave body simulation, the temperatures recorded on the edges of the MRT LBM domain are projected and applied as boundary conditions on the four walls surrounding the red area. A similar procedure is performed for the outer boundary of the mould configuration domain, using the gas temperatures recorded in its vicinity. This one-way coupling allows for different 2D-to −3D conversion methods being applied to the autoclave and mould assembly domains to compute the total heats transferred, as shown in Section 2.4.6.

The MRT LBM simulation is run until thermal equilibrium is achieved within the numerical domain, and a steady-state solution is generated. Thermal equilibrium is defined by a difference between the average gas temperatures in the domain at times t and $t+\Delta t$ of less than the allowed error, δ. This condition is given in Eq. (36):

$$\frac{1}{N_{cells}} \sum_{i=0}^{N_{cells}} \left(T_{i_{t+\Delta t}} - T_{i_t} \right) < \delta \tag{36}$$

where δ [°C] is an arbitrary value chosen by the user. For the simulations performed in this study, a value of $\delta = 1$ [°C] was used. To implement the model computationally, the Python 3.8 programming language was used, together with the NumPy library [29] and the Matplotlib library [30].

2.4.8. Collected experimental data for validation

To validate the model presented in this study, a 0.45 [m] by 0.45 [m] by 0.002 [m] CF/Epoxy prepreg panel was manufactured using autoclave curing. This was done in the Delft Aerospace Structures and Materials Laboratory (DASML) using the case study autoclave described in 2.2. The air temperature in the autoclave was heated at a ramp-up rate of 2 [°C/min] from room temperature to a cure temperature of 120 [°C]. The cure temperature was maintained for a dwell of 90 mins before cooling. This corresponds to the preset temperature used in the simulated models 2.2. The energy consumption of the autoclave during cure was monitored using a power analyser "RS PRO IPM3600N Power Quality Analyser". The monitoring frequency was set at 50 Hz and a reading was recorded every 5 s. These energy readings were compared to the simulated energy consumption results from the proposed models. The result of this comparison is further discussed in 3.3

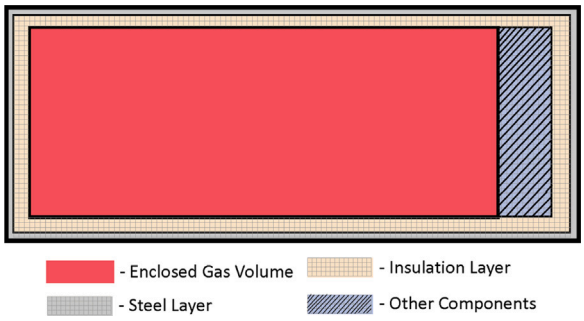

Fig. 8. Square grid mesh of the simplified 2D representation of the autoclave body.

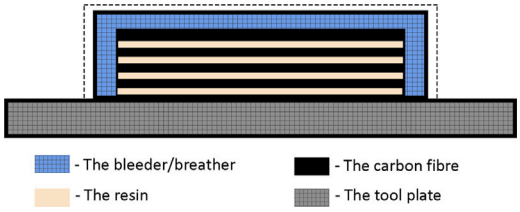

Fig. 9. Sketch of the 2D square grid mesh used to discretize the mould assembly containing the CFRP panel.

3. Results

In this chapter, two simulated energy graphs were produced through the aforementioned methods, using the autoclave and mould parameters from Table 1 and the preset temperature of the cycle. Consequently, the cumulative energy consumption graphs generated from the two models were compared against the experimental energy log for validation.

3.1. Simulated energy consumption using analytical model

This analytical model proposed in Section 2.3 has been used to provide a direct prediction of the most significant heat contributions to the energy consumption of an autoclave cure cycle. The models were applied to the set of inputs given in Table 1, which were obtained from the case study autoclave cycle described in Section 2.2. The autoclave body transferred heat, together with the heat loss to the environment and the heat consumed by the enclosed gas and mould assembly, were determined as functions of time for the case study cure cycle. As shown in Fig. 10, the simulated total energy consumption is 21.1 [kWh], and it is composed of the heat transfer to the autoclave body of 11.3 [kWh], a heat loss to the environment of 8.1 [kWh] and heat transferred to the circulated air of 1.2 [kWh]. Heat transferred to the mould assembly was only 0.4 [kWh].

3.2. Simulated energy consumption with MRT LBM model

The simulation of the energy consumed by the TU Delft autoclave using the MRT LBM method required several more inputs than the analytical method and produced a series of intermediary results required

Table 3
Summary of the input parameters used for the body heat flow simulation of the TU Delft autoclave.

Simulation parameters	Values and units
Spatial Discretization Step	0.015 m
Time Discretization Step	0.01 s
2D Domain Length	3.4 m
2D Domain Width	1.55 m
Auto. Mass	1102 kg
Auto. Total Volume	6.2 m^3
Auto. Inner Volume	4.5 m^3
Auto. Surface Area	13.84 m^2
Auto. Specific Heat Capacity	459.7 – 567.5 J/kg K
Auto. Thermal Conductivity	1.2 W/mK
Auto. Wall Thickness	0.14 m
Ambient Air Temperature	20 °C
Ambient Air Density	1.225 kg m^3
Ambient Air Viscosity	$1.81 \cdot 10^{-5}$ Pa s
Gas Viscosity	$1.81 \cdot 10^{-5}$ Pa s
Gas Specific Heat	1040 J/kg K

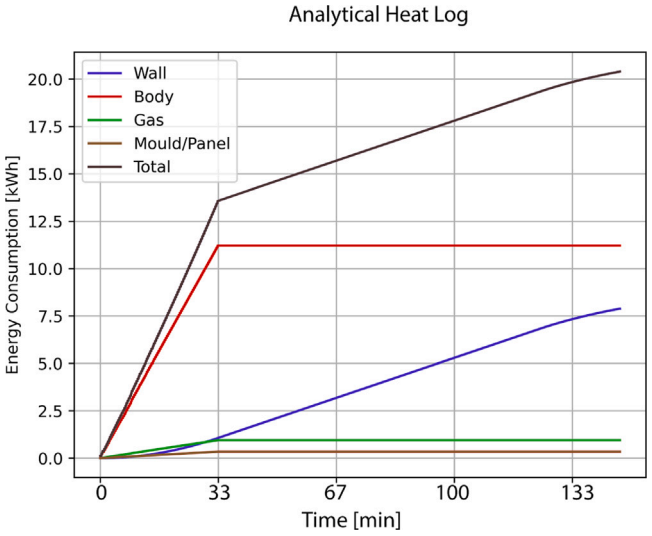

Fig. 10. The autoclave total energy consumption and individual contributions using the simple, analytical method proposed in Section 2.3. The simulation is performed on the cycle in Fig. 2. The final energy consumption of the cycle is 21.1 [kWh].

for the final simulated energy consumption. These are presented below. The first set of results comes from the MRT LBM gas simulation. For this, the simulation inputs given in Table 2 were used. The steady-state temperature field is shown in Fig. 11. As it can be observed in the image, a gradient of decreasing temperature forms in the vicinity of the walls of the autoclave, and a variation in the inner-surface temperature of the walls is noticeable. Next, the temperature at the boundaries of the 2D domain corresponding to the autoclave wall was recorded, to be mapped onto a domain of a different, more simplistic shape, used for the solid heat flow simulation. These temperature fields were used as transient Dirichlet boundary conditions in the simulation, applied at the four sides of the domain. This simulation utilized a different set of parameters, which is given in Table 3. Based on this information, the temperature field within the domain was simulated for the entire duration of the cure cycle, and the heat transfer through it was calculated. A frame of this simulation is shown in Fig. 12, during the dwell time of the cycle. As shown, for a temperature of 110 °C at the inner surface of the domain, temperatures between 25 °C and 65 °C are observed at the outer edges. This implies that the domain is effectively containing the heat produced during the cycle, as the insulator layer of a real autoclave would.

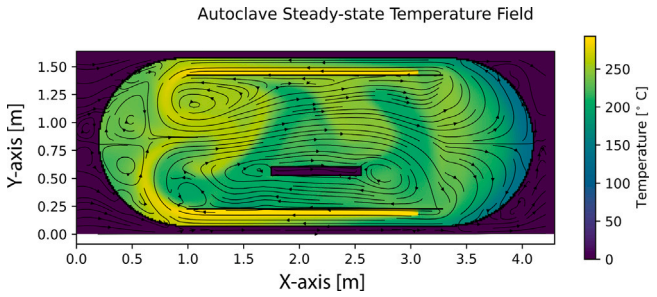

Fig. 11. Steady-state solution of the MRT LBM temperature field simulation at a preset temperature of 120 °**C**, with a fan horizontal nitrogen gas velocity of 6 **m/s**. The temperatures outside the autoclave and inside the mould are set to 20° C. The external boundaries simulate the wall heat loss to the environment.

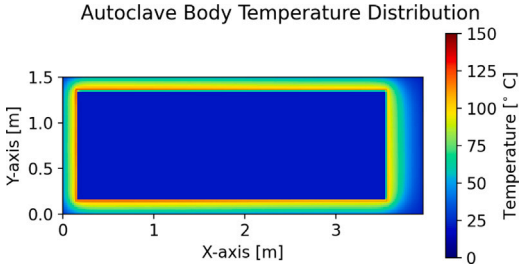

Fig. 12. Transient solution of the Fourier Heat Equation applied to the 2D discretized domain of the autoclave body at a preset temperature of 120 °**C**. The inner boundaries have Dirichlet conditions set to the nitrogen gas temperature, while the outer surface has a convective boundary condition.

Table 4
Summary of the input parameters used for the CFRP mould configuration heat flow simulation.

Simulation parameters	Values and units
Spatial Discretization Step	0.015 m
Time Discretization Step	0.05 s
2D Panel Domain Dim.	0.45 × 0.012 m
2D Bleeder Domain Dim.	0.7 × 0.025 m
2D Tool Plate Domain Dim.	0.9 × 0.009 m
CFRP Number of Layers	12 –
Fibre Mass	0.48 kg
Fibre Specific Heat	675–833 J/kg K
Fibre Thermal Conductivity	153–189 W/mK
Resin Mass	0.205 kg
Resin Specific Heat	1665–2055 J/kg K
Resin Thermal Conductivity	0.09–0.11 W/mK
Bleeder Mass	0.242 kg
Bleeder Specific Heat	1350 J/kg K
Bleeder Thermal Conductivity	0.5 W/mK
Tool Plate Mass	12.15 kg
Tool Plate Specific Heat	921 J/kg K
Tool Plate Thermal Conductivity	200 W/mK
Gas Viscosity	$1.81 \cdot 10^{-5}$ Pa s
Gas Specific Heat	1040 J/kg K

In parallel to this simulation, a second one was run for the heat transfer through the mould configuration, using the same method, and a 2D domain as depicted in Fig. 9. For this simulation, the numerical inputs in Table 4 are used. A frame of this simulation is depicted in Fig. 13, where the temperature field variation within the mould configuration is shown. As it can be seen, the simulated CFRP panel seems to heat up from the edges to the centre, and shows a temperature gradient from 120 [°C] to 90 [°C].

With the autoclave body, mould configuration and gas heat simulations performed, the prediction for the energy log of the MRT LBM model was calculated. This is shown in Fig. 14, where the total energy consumption, as well as its main components, are plotted against time.

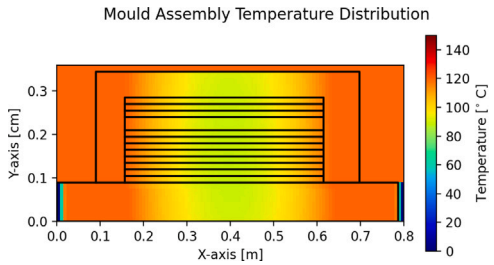

Fig. 13. Transient solution of the Fourier Heat Equation applied to the 2D discretized domain of the mould assembly at a preset temperature of 120 °C. The surfaces of the mould have convective boundary conditions with the nitrogen gas in the autoclave.

The same three phases of the cure cycle that were observed in the analytical model results, can also be noticed here: the heating phase, the dwell phase and the cooling phase. However, the energy variation in time simulated with this method seems smoother than the previous results. This is likely due to the damping introduced by simulating the insulation layer of the autoclave using the 2D Fourier Heat Equation. The simulated total consumed energy falls within a final range of 15.9 [kWh] to 19.02 [kWh] with an average value of 17.47 [kWh]. The upper and lower estimates are based on the input ranges in Tables 3 and 4. The contributing components include the heat transferred to the autoclave body of 13.2 [kWh], heat lost to the environment through convection of 3.9 [kWh] and heat transferred to the mould configuration and gas, of 0.2 [kWh]. An additional component computed by this model is the heat lost through radiation, which was predicted to be 0.2 [kWh] as well. Overall, these results are lower than those predicted by the analytical model. This is most likely due to the use of more detailed temperature fields instead of average values in the computation of heat flows.

3.3. Energy consumption models validation

A quantitative validation of the proposed mathematical models has been done through a comparison between their resulting simulated energy logs and the experimental energy log data described in Section 2.4.8. The result of this comparison is shown in Fig. 15, where three curves are plotted. The experimental energy log in red, the analytical model-produced energy log in dotted black, and the MRT LBM-produced energy log in continuous black. The plot shows a high correlation between both models and the experimental data. For the analytical model, a correlation coefficient of $R^2 = 0.8$ is computed with a 14% overestimation between the simulated and measured energy consumption. On the other hand, the MRT LBM model shows a correlation coefficient of $R^2 = 0.95$, with a 0.03% over estimative difference between the simulated and the experimental results.

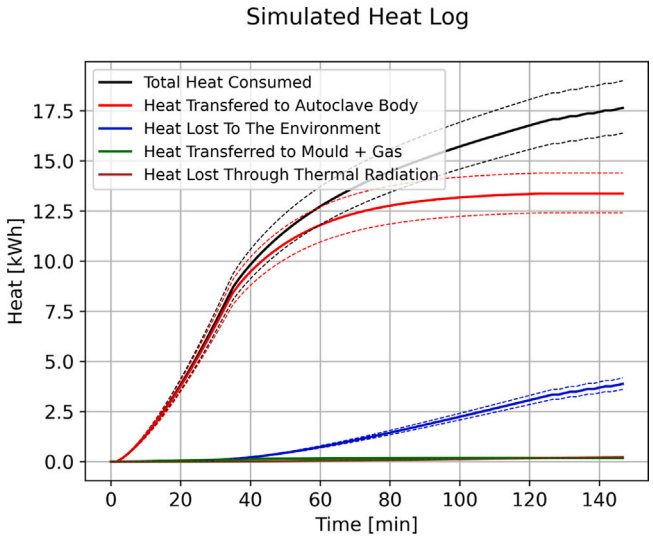

Fig. 14. Simulated heat flows within the autoclave-environment for the CFRP cure cycle. The black lines show total simulated heat consumption of the autoclave. The green line shows heat transferred to the mould assembly and gas, red lines show heat flow to the autoclave structural body, blue lines show the heat lost through the outer walls to the environment. The brown line shows the heat lost through radiation to the environment.

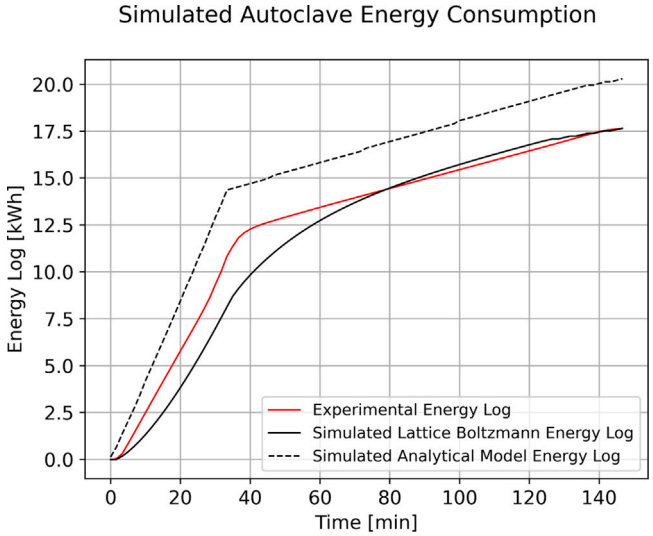

Fig. 15. Simulated vs. recorded total energy logs of the autoclave cure cycle. The continuous line represents the simulated log using the Lattice Boltzmann-based method, while the dotted line represents the log computed with the analytical method.

4. What-if analysis

One major benefit of the proposed models is that they can be used to predict energy consumption of an autoclave with varying process parameters. This section assesses how variations in selected process parameters can influence energy consumption of autoclave curing.

4.1. Varying autoclave loading capacity

Autoclaves used for curing composites are cylindrical pressure vessels and come in various sizes. In industrial applications, batch manufacturing of composite parts is common as it saves time and manufacturing cost. However, an autoclave can only run one cure cycle at a time. This implies that only parts with the same cure cycle can be run together at the same time. This can pose a challenge especially for large autoclaves as often times they are not loaded to their maximum capacity. Hence, this section analyses how energy consumption of an autoclave is affected by change in panel size. To achieve this, the maximum part length and width that can be cured at a time, in the case study, was used. In order to simulate the energy consumption, the two heat transfer models were used — MRT LBM and analytical method. The energy consumption of the autoclave has been observed by changing the dimensions of the panel. The results have been compiled by running the method discussed in Section 2. The following assumptions were made regarding the cured panel. First, the panel is assumed to be a rectangular panel with a constant laminate thickness of 2 [mm]. Then, the composition of the panel is assumed to be homogeneous, making the density of the panel constant. Furthermore, the part tool is assumed to be a rectangular aluminium tool plate with a constant thickness of 1.8 [mm], and the dimensions of the tool are increased linearly with

Table 5
Estimated energy consumption with respect to variation in panel area using MRT LBM and analytical model.

Length and width [m × m]	Area [m^2]	Energy consumption for MRT-LBM [kWh]	Energy consumption for analytical model [kWh]
1.080 × 1.700	$1.83 * 10^{0}$	18.8411	22.6114
0.540 × 0.850	$4.59 * 10^{-1}$	18.3082	20.2732
0.270 × 0.425	$1.14 * 10^{-1}$	18.1749	19.6887
0.1350 × 0.2125	$2.87 * 10^{-2}$	18.1416	19.5426
0.0675 × 0.1063	$7.17 * 10^{-3}$	18.1333	19.5060
0.03375 × 0.05312	$1.79 * 10^{-3}$	18.1312	19.4969
0.01687 × 0.02656	$4.48 * 10^{-4}$	18.1307	19.4946
0.00844 × 0.01328	$1.12 * 10^{-4}$	18.1306	19.4940

the dimensions of the panel. Finally, the material composition (carbon Fibre/Epoxy) and temperature cycle used are same with that of the case study part as defined in Section 2.2.

4.2. Varying panel dimensions

For this analysis, the laboratory-scaled autoclave was first assumed to be loaded to its maximum capacity, which is the maximum area of a panel that can be cured at a time. According to the manufacturer's data sheet, the maximum area of the panel is 1.08 × 1.7 [m^2]. It was assumed that the volume of the autoclave is small and will not allow for vertical stacking of additional parts, hence this was not considered.

Then the panel size was varied within the autoclave and the total electrical energy consumption was estimated. To achieve this, the panel areal dimensions (length and width) were decreased using geometric progression with a common ratio of 2 until a selected minimum panel size of 0.00844 [m] × 0.01328 [m] was attained. Table 5 contains the estimated energy consumption of the autoclave with respect to different panel dimensions from the MRT LBM and analytical methods.

As seen in Table 5 and Fig. 17, although the area of the CFRP part was varied in three orders of magnitude, the estimated energy consumption was approximately the same for MRT LBM with a difference in the energy consumption for the largest and smallest panel being 3.77%. However, in case of analytical method, the change in energy consumption is 15.34%. Also, after the panel area becomes smaller than a certain area which is 0.114 [m^2] in this case, the energy consumption remains more or less the same for both models. This shows that the total energy consumption of the autoclave does not change significantly when its loading capacity is varied or when composite and mould dimensions are changed, especially for small panel sizes. This is consistent with the two models. Although the total energy consumption does not vary significantly with variations in loading capacity, the specific energy attributed to each cured part varies considerably, as shown in Fig. 17

The values of the energy consumption in Table 5 were estimated considering the maximum length and width of a panel that the case study autoclave can cure at a time. Also, only one autoclave stacking layer was considered. Although this gives us insight into the influence of loading capacity on the energy consumption of an autoclave, it limits the autoclave capacity to a 2D rectangular panel without considering the influence of part curvature and stacking layers. In order to consider these factors, more detailed loading models for autoclaves need to be considered, which is outside the scope of our study.

4.3. Effects of cure cycle

Temperature cycle during cure not only determines the microstructural quality of a part [36] but also can influence the energy consumption of the autoclave during cure. This is because the cure cycle determines the cure temperature of a matrix system alongside the ramp-up rate and dwell times, which significantly influences the amount of heating required during cure.

The influence of varying the cure cycle on energy consumption was analysed in this study by first comparing the temperature cycle used in Section 2.1: 120 [°C] cure temperature with ramp up rate of 2 [°C]/min and 90 min dwell time, with an alternative cure cycle for the same panel dimension. This was also specified in the manufacturer data sheet but was not the recommended standard cycle. This alternative cure cycle (130 [°C], 3 [°C]/min ramp up rate and 60 min dwell time) has higher cure temperature and ramp up rate 3 [°C]/min but less dwell time. The results obtained show that the cumulative energy consumption of the alternative cycle was 0.2 [kWh] higher, a difference of approximately 1% (see Fig. 16).

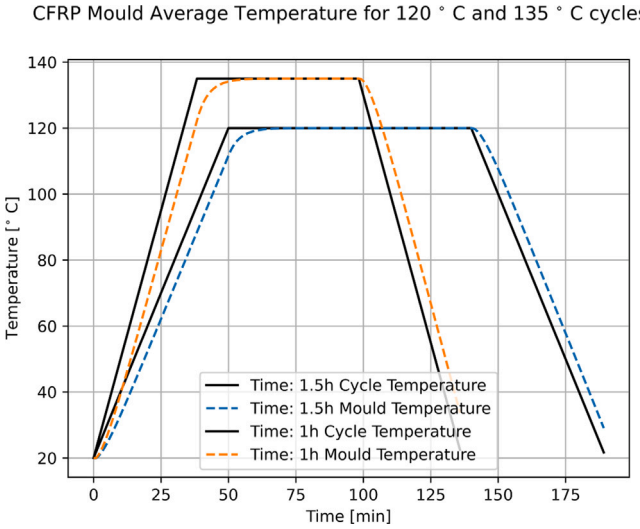

Fig. 16. Temperature responses of the mould assembly to 2 CFRP-curing cycles for "Deltatech GG200T - DT120" prepreg system.

To further investigate the influence of cure cycle, its energy consumption was also compared to cure cycles for other composite materials commonly used in aerospace applications. This includes Hexcel M21, a 180 [°C] epoxy curing matrix system and the Toray Cetex® TC1225 Low Melt PAEK thermoplastic composite. As seen in 19, the estimated energy consumption of Hexcel M21 with a 180 [°C] curing system, summed up to 53 [kWh]. This amounts to a 180% increase in energy consumption when compared to our case study Delta Preg 120 composite (with a 120 [°C] curing system). The estimated energy consumption of the LM PAEK (a thermoplastic with a 320 processing temperature) summed up to 67 [kWh], approximately 3.5 times higher than the energy consumption of the Delta Preg case study part. This analysis shows that energy consumption is sensitive to the cure cycle of a part, mostly influenced by the cure temperature. This is because most of the energy is consumed during ramp up to the cure temperature and not necessarily the dwell time. The energy consumed during dwell is mainly to complement heat loss through the walls or, in some cases, to account for an increase in pressure. Increasing the pressure introduces additional air/nitrogen into the system which need to be heated up, hence consuming additional energy.

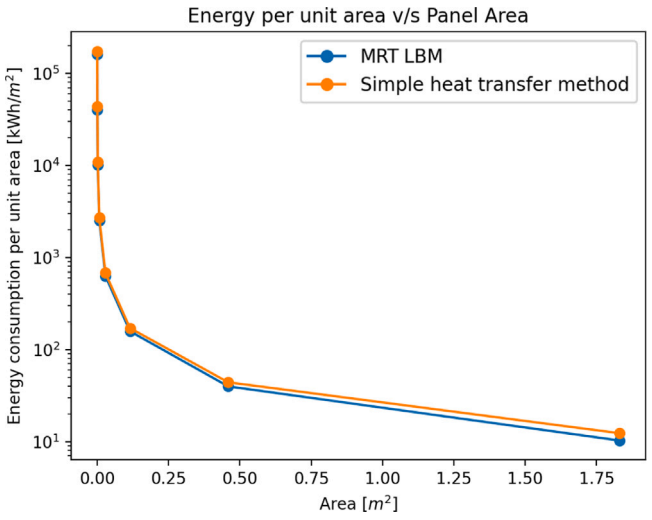

Fig. 17. Energy consumption per unit area of the autoclave with respect to different panel areas.

4.4. Effect of autoclave size

For industrial applications, it is relevant to determine how the energy consumption of an autoclave design scales with a proportional increase in its dimensions. To perform such an analysis, the models outlined in Sections 2.3 and 2.4, together with autoclave design regulations for pressure vessels according to European standard EN 13445 [37]. For this analysis, it was assumed that the autoclave pressure vessel is made out of Stainless Steel 316L. Furthermore, the insulating layer is an Aluminium Oxide Fibre blanket. To determine the necessary thickness of the steel layer of the autoclave, the pressure vessel formula in Eq. (37) is used:

$$s_{Steel} = \frac{SF}{\sigma_y} \cdot p_{cycle} \cdot R_{auto} \tag{37}$$

where SF is the safety factor of 3, R_{auto} is the autoclave radius, p_{cycle} is the cycle maximum pressure and σ_y is the yield strength of the stainless steel structure. This analysis was applied to the real autoclave design, by varying its volume from 5 to 400 [m^3] with multiple intermediate steps.

Fig. 18 shows the variation in estimated energy consumption with autoclave volume for both models. The first conclusion is that the increases in volume cause a relatively linear response in both models, which suggests that the autoclave dimension itself is a major contributor to the energy consumption of the cycle. This can be attributed to the autoclave body, due to more mass, the contained gas due to more inner volume, and the heat loss due to bigger autoclave area.

Consequently, it is essential to note the differences between the two models. The analytical model provides a much higher estimate of energy consumption compared to the MRT LBM model. The difference between the two values is also seen to diverge as the autoclave size increases. This could be due to the analytical model overshooting the heat loss value, the overshoot increases as the autoclave size increases and more heat loss is experienced. Another interesting feature is the different shapes of the cumulative energy curve generated from the proposed models. The analytical model follows simpler curves. Once the temperature stabilizes at around 30 min, only the heat loss through the wall makes an added contribution to the log in the remainder of the cycle. On the other hand, the MRT LBM incorporates the transient behaviour of the system, it does not assume an immediate temperature equilibrium like the analytical model. This makes the contributions delay in time and results in a slower but progressive increase in energy consumed.

Table 6
Heat loss change by varying insulator thickness. Stainless steel structural thickness is fixed at 0.015 [m].

Change	Thickness [m]	Heat loss [kWh]	Difference
Reference	0.085	9.087	Reference
+20%	0.102	8.588	−5.49%
+40%	0.119	8.145	−10.37%
+60%	0.136	7.748	−14.74%
+80%	0.153	7.377	−18.82%
+100%	0.170	7.051	−22.40%

4.5. Varying insulation thermal conductivity and autoclave wall thickness

Heat loss through the autoclave walls contributed significantly to its total energy consumption, as seen in Section 2.4.3. To estimate heat loss, parameters including insulator conductivity, wall thickness, autoclave area and cure temperature were used as expressed in Eq. (3). In this section, the sensitivity of autoclave energy consumption to varying insulator conductivity and wall thickness is assessed. The model for estimating heat flow through the autoclave wall described in Section 2.4.3 was used. Here, the autoclave wall consists of a 0.12 [m] thick aluminium oxide insulation blanket and 0.015 [m] thick stainless steel wall. The insulation thermal conductivity and wall thickness were varied in two scenarios described below, and the resulting heat loss for each scenario was recorded and analysed.

In the first scenario, the arbitrary thickness and conductivity of the structural steel layer were kept constant while the thickness of the aluminium oxide insulation foam were varied. By varying the insulation layer thickness, the total autoclave wall thickness also changed. The heat loss through the autoclave wall is calculated for every insulation layer thickness considered. The result provides an insight as to how varying insulator thickness can influence heat loss and subsequently energy consumption of an autoclave. In the second scenario, the thermal conductivity of the insulation and structural steel materials were varied to see how this affects heat loss. This is possible as different steel alloys or insulator mixtures provide a spectrum of values with the potential of resulting in completely different heat loss values.

4.5.1. Constant steel thickness with varying insulation thickness

The thickness of the insulator for our case study autoclave was varied between 0.03 [m] and 0.23 [m]. This range of values was selected because they are still within the thickness range of the original autoclave configuration (0.12 m). The thermal conductivity of the insulator, which is in our case study autoclave, aluminium oxide foam, was set at 1.1 [W/mK]. This value was obtained from a manufacturer data sheet and extrapolated to account for the current curing cycle [38]. The thermal conductivity of the stainless steel wall was obtained from online website “Engineering Toolbox” [39] and set at 14.4 [W/mK]. With these sets of values, the heat loss through the autoclave wall for varying insulator thickness was estimated and shown in Fig. 21. As seen in Fig. 21, varying the thickness of the insulator layer influenced the heat loss through the walls. However, the effect of increasing insulation thickness progressively decreases as the insulator gets thicker. This is also shown in Table 6.

4.5.2. Varying conductivity of stainless steel and insulator

The conductivity values of the stainless steel structural body of the autoclave and aluminium oxide blanket insulation were varied and the resulting heat loss through the autoclave wall was estimated. While the total thickness and insulation ratio were kept to imitate the case study autoclave setup (0.135 [m] and 88.9%, respectively), the ranges that were chosen for the materials were: 0.935–1.265 [W/mK] for the aluminium oxide blanket (±15% margin from the original value of 1.1 [W/mK]) and 12.24–16.56 [W/mK] (±15% margin from the original value of 14.4 [W/mK]) for the stainless steel.

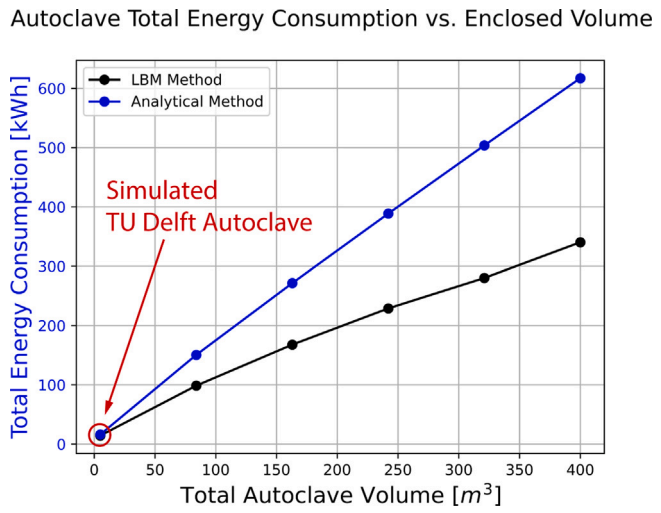

Fig. 18. Total simulated energy consumption for a 120 °C thermoset cycle using the Lattice Boltzmann-based method (continuous lines) and the analytical (simple) method (dotted lines) for different autoclave volumes.

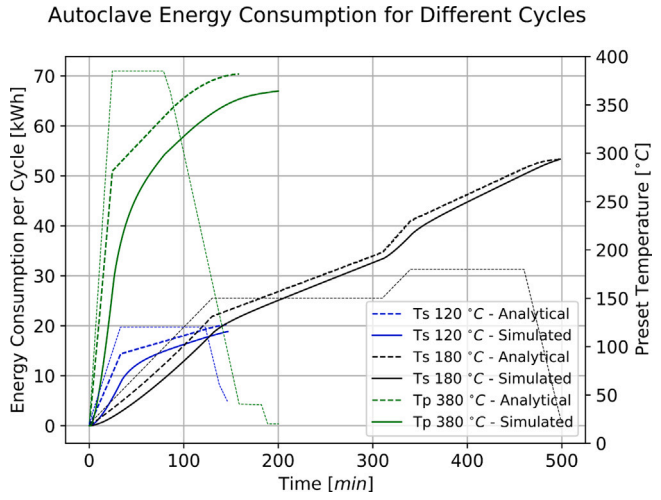

Fig. 19. Energy logs for 3 CFRP-curing cycles applied to a laboratory-scaled autoclave.

Table 7
Heat loss changes as a result of altering insulator thermal conductivity values in a range of 15% of the original value, while keeping steel conductivity constant at 14.4 [W/mK].

Change	Ins. Con. [W/mK]	Heat loss [kWh]	Difference
−15.0%	0.935	7.620	−6.16%
−7.50%	1.018	7.888	−2.86%
Reference	1.100	8.120	Reference
7.50%	1,183	8.332	2.61%
15.0%	1.265	8.526	5.00%

Tables 7 and 8 show the changes in estimated energy consumption by varying the insulator and steel thermal conductivities. These tables show that varying the conductivity of the insulator material affect the heat loss much more significantly than varying the conductivity of the stainless steel body. For instance, in Tables 7 and 8, a change of 7.5% to the original insulator conductivity creates a 3% increase in heat loss, while a change of 7.5% in the original steel conductivity merely changes the heat loss by 0.02%.

The perspectives provided by the two different scenarios in Tables 6 and 7 show that heat loss is sensitive to thermal conductivity and thickness of the insulating material. The results also show that the heat loss through the autoclave wall is more sensitive to the thickness of the insulation than it is to its conductivity.

Table 8
Heat loss changes as a result of altering stainless steel thermal conductivity values in a range of 15% of the original value, while keeping insulator conductivity constant at 1.1 [W/mK].

Change	Steel Con. [W/mK]	Heat loss [kWh]	Difference
−15%	12.24	8.115	−0.061%
−7.5%	13.32	8.118	−0.028%
Reference	14.40	8.120	Reference
7.5%	15.48	8.122	0.024%
15%	16.56	8.124	0.045%

5. Discussion

In this study, two mathematical models were proposed to predict the energy consumption of autoclave curing in CFRP manufacturing. An analytical model based on Fourier heat equations and an MRT LBM based model. This section compares the two methods taking into account the differences in the simulated energy consumption results, reasons for these differences, possible applications and limitations of each model.

5.1. Models comparison and possible applications

The two models presented in this study have a few similarities. They are both 2D models that take into account thermal diffusion and convection. They both utilize thermodynamics based heat equations to estimate heat flow through the solid mediums (e.g. wall) and solid fluid boundaries. Also, they both estimate total energy consumption and discriminate this consumption to the different elements of autoclave curing. Despite these similarities, the results obtained from these methods differed by 11% and this is attributed to the main difference between them.

The main difference between these models is that the analytical model assumes an averaged temperature equivalent to the predetermined cure temperature cycle. The MRT LBM method, on the other hand, simulates the transient velocity and temperature variation of the flowing gases within the autoclave. Which is then used to estimate temperature variations on the solid boundaries (mould assembly and autoclave structure). Neglecting this temperature variation can lead to an overestimation of the heat loss through the walls and subsequently the total energy consumption. Amongst the two methods considered, the estimated energy consumption from the MRT LBM method had a closer match to the experimental data, with only a 1% difference (see Fig. 20).

Another difference between the two models is that the MRT LBM method considers heat transfer due to thermal radiation. This value is relatively small and accounts for only 1% of the simulated energy consumption. Another interesting feature is the different shapes of the energy curves, as seen in Fig. 15. The analytical model follows simpler curves: once the temperature stabilizes at around 30 min, only the heat loss through the wall makes an added contribution to the log in the remainder of the cycle. On the other hand, the MRT LBM incorporates the transient behaviour of the system, it does not assume an immediate temperature equilibrium like the analytical model. This makes the contributions delay in time and results in a slower but progressive increase in energy consumption until temperature equilibrium is attained.

Although the energy consumption values estimated by the two models differed by 11%, the what-if analysis carried out in this study shows that as the autoclave increases, the variations in the results from the two methods increases 4.4. This is attributed to the increased autoclave dimensions and higher insulator thickness. With larger autoclave dimensions, the temperature variation at the walls is much more

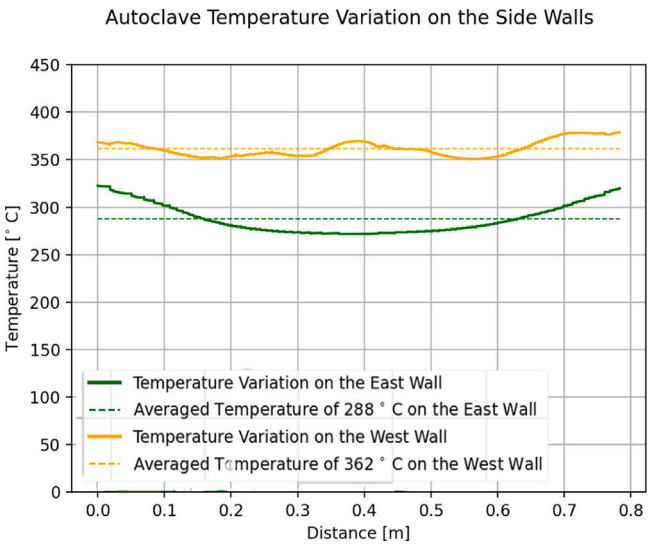

Fig. 20. Temperature variation at the wall of an autoclave, represented by the MRT LBM Method at a 400 [°C] temperature cycle. At 400 [°C], the temperature on the east wall averaged 288 [°C] and 362 [°C] on the West wall.

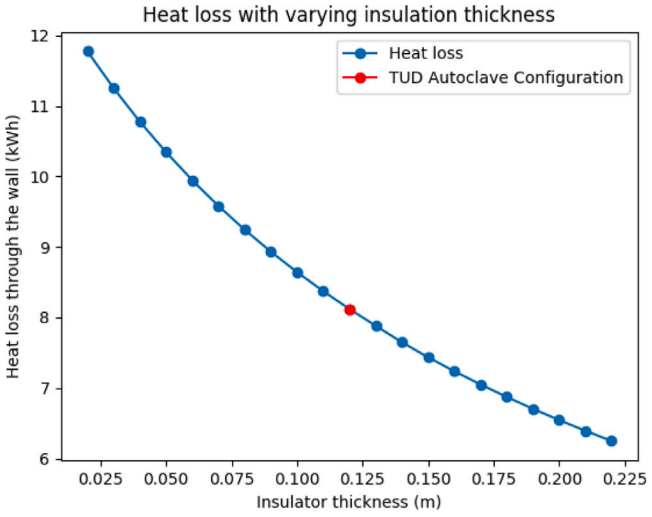

Fig. 21. The heat loss with constant structural and varying insulation thickness. The steel layer has a thickness of 0.015 [m]. TU Delft autoclave configuration shown in red. This was estimated using the analytical method.

significant. Also, by increasing the insulation thickness, the diffusion of heat through the autoclave wall slows down, hence the temperature field reaches steady state at a shorter amount of time. Since the analytical model does not account for temperature variation and diffusion at the autoclave walls, the resulting energy consumption would be overestimated significantly.

One major benefit of the analytical model over the MRT LBM model is its lower computational effort. This makes it suitable for applications where only rough estimates of total energy consumption are needed. This may be the case in some energy cost estimations or what-if analysis The MRT LBM method, although with a higher computational effort, has some benefits. It provides more accurate results and can estimate energy consumption at high frequency throughout the cure cycle (i.e. energy consumption for every selected time step, say 5 seconds interval). This makes it suitable for applications where more precise energy logs are needed or applications requiring energy monitoring at higher frequencies. This may be the case when comparing cure cycles in terms of energy efficiency.

The models presented in this study do have some limitations. One major limitation is that both models represent the autoclave as a 2D computational domain, which is not the case with an autoclave. However, in the MRT LBM based model, the heat flow occurring in the 2D domain of the autoclave body and the mould assembly were converted to 3D outputs to provide results that are more representative. The heat flow conversion for the autoclave body and mould assembly were done using different methods, considering their differences in axial symmetry. The conversion for the mould was simplified based on the assumption that the through width temperature variation of the mould assembly is negligible. This can also be seen as a limitation. The MRT LBM based model also assumes no reverse dependency between the mould and the autoclave domains during expansion, hence allows different expansion methods to be used.

Another limitation is that the models require some preset temperature cycle, which is obtained empirically. In most cases this can be found in a manufacturer data sheet of the prepreg or resin materials, but this dependency on empirical data is still a limitation. It is important to note that this study covers energy consumption of the autoclave for only heating and air circulation within the autoclave. Autoclave curing also incurs other energy demands, including energy for producing Nitrogen gas (in some cases, air is used instead to eliminate this demand), energy for pumping the gas into the autoclave and cooling. These aspects were out of scope and not considered in this study.

6. Conclusion

This work presents two mathematical models for estimating energy consumption of an autoclave during composite curing. An analytical model based on Fourier heat equations and an alternative model that combines Fourier laws with 2D MRT LBM. The major difference between these two methods is that the MRT LBM model takes into account the temperature gradient occurring within the autoclave and at the autoclave walls, while the analytical model assumes an average temperature value. The simulated energy consumption results were compared to an energy log from the case study experiment carried out in a 4.5 [m^3] autoclave at Delft University of Technology. The MRT LBM method predicted a value range between 15.9 [kWh] to 19.04 [kWh] with an average value of 17.47 [kWh]. The average value 17.47 [kWh] is only 1% lower than the recorded value, indicating a better match. However, one advantage of the analytical model over the MRT LBM model is its lower computational effort, as the MRT LBM method takes a longer time to run and require more detailed information about the autoclave curing process. This can be beneficial in some applications where rough estimates of energy consumption and not precise values are required, and may be the case for some energy cost estimations and sensitivity analysis.

The two models presented in this study have three main advantages. They are parametric, scalable and can segregate the energy consumption of the autoclave curing process. In this study, the autoclave energy consumption was segregated into heat flow to the autoclave body, the composite-mould part, the nitrogen gas and heat loss through the autoclave walls. The results show that heat flow to the mould assembly and the nitrogen gas combined only accounted for less than 2% of the total energy consumption. This implies that the efficiency of the autoclave is significantly low, as the energy consumed for the curing process itself constitutes only 1.1%. It also suggests that existing autoclave designs are developed for curing efficiency, rather than energy-efficiency, and from an energy-efficiency point of view significant improvements still need to be made.

Their adaptability to changing process parameters allows the models to identify those design/process parameters that significantly influence the energy consumption of an autoclave. As seen in the what-is

analysis carried out in this study, the temperature cycle and autoclave volume are the most influential parameters, followed by the insulation thickness and conductivity. Identifying these parameters provides insight as to possible design and process changes that may improve autoclave energy efficiency. This can serve as a guide to future energy reduction target for autoclave curing. The scalability of the models allows energy consumption results obtained using pre-defined cure cycle, to be scaled up for production scenarios such as autoclave size and autoclave loading (loading it to full capacity or not). This element may be essential in prospective life cycle assessment studies where lab scale experiments are scaled up to be more representative of future industrial scale scenarios [40]. It may also be valuable in cost models for predicting possible energy cost for different scales of production [41].

In general, these models provides better access to energy inventory that can serve as input in cost models for estimating energy costs and in LCA studies. This is needed especially in the aerospace industry, where most data required for these studies are proprietary and not readily available.

To further develop these models for better accuracy, a few more steps are recommended. It is recommended to apply the two models to a wider range of cure cycles and autoclaves for more validation. The analytical model can further be developed by including a correction factor or additional equations to account for temperature variations within the autoclave. Also, extending the MRT LBM model to have 3D simulations that better represent the autoclave as a computational domain, may be beneficial in getting more accurate results.

CRediT authorship contribution statement

Chizoba J. Ogugua: Conceptualization, Writing – original draft and editing, Data curation, Methodology, Validation, Analytical method and what-if analysis. **Sabin V. Anton:** Writing – original draft and editing, Software, Visualisation, Methodology, MRT LBM method and what-if analysis. **Aditya P. Tripathi:** Writing – original draft, Visualisation, Methodology, What-if analysis. **Miguel Dominguez Larrabeiti:** Writing – original draft, Software, Visualisation, Methodology, Analytical method and what-if analysis. **Sean O. van Hees:** Writing – original draft, Visualisation, Methodology, What-if analysis. **Jos Sinke:** Conceptualisation, Writing – review & editing, Supervision. **Clemens A. Dransfeld:** Conceptualization, Writing – review & editing, Supervision, Funding acquisition.

Declaration of competing interest

The authors declare that they have no known competing financial interests or personal relationships that could have appeared to influence the work reported in this paper.

Data availability

I have shared the link to the code used in the study. The link was referenced in the manuscript. I also uploaded a .csv file with data used for the plots. Please feel free to contact the correspondent.

Acknowledgements

The work presented in this paper is part of the EDEN project (Ecolonomic Design EvolutioN) with funding from Fraunhofer Gesellschaft, Netherlands under grant agreement No. L20802. The results and conclusion presented in this paper are those of the authors only and do not represent the position of Fraunhofer Gesellschaft.

The Authors would like to acknowledge Berthil Grashof and other technicians at the Delft Aerospace Structures & Materials Laboratory (DASML) for their support in data collection.

Appendix A. Supplementary data

Supplementary material related to this article can be found online at https://doi.org/10.1016/j.compositesa.2022.107365.

References

[1] Drakonakis V, Seferis J, Doumanidis C. Curing pressure influence of out-of-autoclave processing on structural composites for commercial aviation. Advant Mater Sci Eng 2013;2013(356824):14. http://dx.doi.org/10.1155/2013/356824.

[2] Mirzaei S, Krishnan K, Kobtawy A, Roberts J, Palmer E. Heat transfer study and optimization of autoclave system in composites manufacturing. In: IIE annual conference. 2020, p. 405–10.

[3] Witik R, Gaille F, Teuscher R, Ringwald H, Michaud V, Månson J-A. Asessing the economic and environmental potential of out of autoclave processing. In: 18th International conference on composite materials. 2011, p. 1–5.

[4] Antonucci V, Giordano M, Inserraimparato S, Nicolais L. Analysis of heat transfer in autoclave technology. J Reinf Plast Compos 2001;22:613–20.

[5] Seow Y, Rahimifard S. A framework for modelling energy consumption within manufacturing systems. CIRP J Manuf Sci Technol 2011;4(1):258–64.

[6] Vita A, Castorani V, Germani M, Marconi M. Comparative life cycle assessment and cost analysis of autoclave and pressure bag molding for producing CFRP components. Int J Adv Manuf Technol 2019;105:1967–82.

[7] Katsiropoulos C, Loukopoulos A, Pantelakis S. Comparative environmental and cost analysis of alternative production scenarios associated with a helicopter's canopy. Aerospace 2019;6(1). http://dx.doi.org/10.3390/aerospace6010003.

[8] Wang Q, Wang L, Zhu W. Design optimization of moulds for autoclave process of composite manufacturing. J Reinf Plast Compos 2017;36:1564–76.

[9] Wang L, Zhu W, Wang Q. A heat-balance method for autoclave process of composite manufacturing. J Compos Mater 2019;53:641–52.

[10] Xie G, Liu J, Zhang W, Sunden B. Simulation and thermal analysis on temperature fields during composite curing process in autoclave technology. In: Proceedings of the ASME 2012 international mechanical engineering congress and exposition, Vol. 7: Fluids and Heat Transfer. 2012, p. 1–9.

[11] Bohne T, Frerich T, Jendrny J, Jurgens J. Simulation and validation of air flow and heat transfer in an autoclave process for definition of thermal boundary conditions during curing of composite parts. J Compos Mater 2018;52.

[12] Zhao F, Xiao H, Vahdati M. Evaluation of spalart-allmaras turbulence model forms for a transonic axial compressor. 2020.

[13] Zhu J, Frerich T, Herrmann A. CFD modeling and validation of heat transfer inside an autoclave based on a mesh independency study. J Compos Mater 2021;55.

[14] Witik R, Teuscher R, Michaud V, Ludwig C, Månson J. Carbon fibre reinforced composite waste: An environmental assessment of recycling, energy recovery and landfilling. Composites A 2013;49:89–99.

[15] Zhang C, Wang Y, Liang X. Research with CFX software on frame mould temperature field simulation in autoclave process. Polym Compos 2009;17:325–36.

[16] Hu J, Zhan L, Yang X, Shen R, He J, Peng N. Temperature optimization of mold for autoclave process of large composite manufacturing. J Phys Conf Ser 2020;1549(3):032086. http://dx.doi.org/10.1088/1742-6596/1549/3/032086.

[17] Kluge J, Lundström T, Westerberg L, Nyman T. Modelling heat transfer inside an autoclave: Effect of radiation. J Reinf Plast Compos 2016;35(14):1126–42.

[18] Cruz-Cruz I, Ramírez-Herrera C, Martínez-Romero O, Castillo-Márquez S, Jiménez-Cedeño I, Olvera-Trejo D, et al. Influence of epoxy resin curing kinetics on the mechanical properties of carbon fiber composites. Polymers 2022;14(6):1100. http://dx.doi.org/10.3390/polym14061100.

[19] CKN KPC - Knowledge in Practice Center. Polymer properties, heat of reaction. 2021, https://compositeskn.org/KPC/A114. [Accessed 20 September 2022].

[20] Xie J, Zhou X, Wu J, She C, Feng C. Mechanism of curing behavior for CFRP compression molding under thermo-mechanical-chemical multi-field coupling. Rev Mater 2022;27(3):9–10. http://dx.doi.org/10.1590/1517-7076-RMAT-2022-0108.

[21] Dong C, Zhou J, Ji X, Yin Y, Shen X. Study of the curing process of carbon fiber reinforced resin matrix composites in autoclave processing. Procedia Manuf 2019;37(1):450–8. http://dx.doi.org/10.1016/j.promfg.2019.12.073.

[22] Yang F, Shi X, Guo X, Sai Q. MRT lattice Boltzmann schemes for high Reynolds number flow in two-dimensional lid-driven semi-circular cavity. Energy Procedia 2012;16:640–1.

[23] Anton S, Larrabeiti M. Encon: Estimating energy consumption of an autoclave using thermodynamics based semi-empirical models, v1.0, Zenodo. 2022, http://dx.doi.org/10.5281/zenodo.6581294, https://github.com/tud-amt/encon-ac.

[24] Berenberg B. Improving autoclave performance. 2003, https://www.compositesworld.com/articles/improving-autoclave-performance.

[25] Hubert P, Centea T, Grunefelder L, Nutt S, Kratz J, Levy A. Out-of-autoclave prepreg processing. In: Comprehensive composite materials II. Elsevier Ltd.; 2018, p. 63–94, Ch. 2.4.

[26] Guillard H, Nkonga B. Thermal modeling, analysis, and design. In: Modeling, analysis, design, and tests for electronics packaging beyond Moore. Chemical Industry Press Co., Ltd.; 2019, p. 63–4, Ch. 3.
[27] Tosun I. Evaluation of transfer coefficients: Engineering correlations. Model Transp Phenom 2007;90–101.
[28] Incropera F, DeWitt D, Bergman T, Lavine A. Fundamentals of heat and mass transfer. 6th ed.. John Wiley & Sons; 2007.
[29] Harris CR, Millman KJ, van der Walt SJ, Gommers R, Virtanen P, Cournapeau D, et al. Array programming with NumPy. Nature 2020;585(7825):357–62. http://dx.doi.org/10.1038/s41586-020-2649-2.
[30] Hunter JD. Matplotlib: A 2D graphics environment. Comput Sci Eng 2007;9(3):90–5. http://dx.doi.org/10.1109/MCSE.2007.55.
[31] Torres M, Collombet F, Douchina B, Crouzeixa L, Grunevaldb YH, Lubinc J, et al. Monitoring of the curing process of composite structures by tunnelling junction sensors. Sensors Actuators A 2015;235(8):256–64.
[32] Guillard H, Nkonga B. On the behaviour of upwind schemes in the low mach number limit: A review. In: Handbook of numerical analysis. Elsevier B.V.; 2017, p. 203–31, Ch. 8.
[33] Bao Y, Meskas J. Lattice Boltzmann method for fluid simulations. 2014.
[34] White F. Viscous fluid flow. 1991.
[35] Piccinno F, Hischier R, Seeger S, Som C. From laboratory to industrial scale: Ascale-up framework for chemical processes in life cycle assessment studies. J Clean Prod 2016;135:1085–97.
[36] Gomarasca S, Peeters D, Atli-Veltin B, Dransfeld C. Characterising microstructural organisation in unidirectional composites. Compos Sci Technol 2021;215(109030).
[37] Lidonnici F, Baylac G, Cannerozzi M, Decock J, Fawcett R, Handtschoewercker A, et al. Unfired pressure vessels. Background to the rules in part 3 design, no. 2 in 16528. Union de Normalisation de la Mécanique; 2004.
[38] Advanced-Ceramic-Materials. AC2468 alumina foam insulation, aluminum oxide foam insulation. 2020, https://www.preciseceramic.com/products/alumina-ceramic-foam-insulation/.
[39] Engineering-Toolbox. Thermal conductivity of metals, metallic elements and alloys. 2005, https://www.engineeringtoolbox.com/thermal-conductivity-metals-d_858.html.
[40] Miller S, Keoleian G. Framework for analyzing transformative technologies in life cycle assessment. Environ Sci Technol 2015;49(5):3067–75.
[41] Song Y, Youn J, Gutowski T. Life cycle energy analysis of fiber-reinforced composites. Composites A 2009;40(8):1257–65.